Journal of Translational Medicine

RESEARCH

Open Access

RBX1 mitigates ferroptosis by inhibiting NCOA4-mediated ferritinophagy and contributes to the attenuation of intervertebral disc degeneration

Lu-Ping Zhou[1,2,3†], Liang Kang[1,2,3†], Zhi-Gang Zhang[1,2,3†], Chong-Yu Jia[1,2,3], Chen-Hao Zhao[1,2,3], Xian-Liang Zhang[1,2,3], Hua-Qing Zhang[1,2,3], Ren-Jie Zhang[1,2,3*] and Cai-Liang Shen[1,2,3*]

Abstract

Loss of nucleus pulposus (NP) cells is as one of the primary factors initiating intervertebral disc (IVD) degeneration (IVDD); however, the intrinsic physiological mechanisms of endogenous NP-derived stem cell (NPSC)-based therapy in IVDD remain poorly understood. Disturbed iron homeostasis is commonly observed in degenerative diseases, and an acidic microenvironment has been considered a crucial factor in IVDD. The molecular mechanism of ferroptosis in acidic microenvironments during IVDD has not been reported. Herein, we intended to investigate whether acidic conditions can induce ferroptosis in NPSCs and explore the mechanism of IVDD progression through NCOA4-mediated ferritinophagy, which is a type of selective autophagy mediating ferroptosis. The role of ring-box 1 (RBX1) in NCOA4-mediated ferritinophagy in NPSC ferroptosis and IVDD pathogenesis was also explored. First, clinical epidemiology research revealed that a reduction in serum ferritin level was an independent risk factor for IVDD. We then demonstrated that ferroptosis progressively increased in human NP tissues as IVDD advanced and the acidic conditions induced ferroptosis-associated decline in cell viability, reactive oxygen species accumulation, and extracellular matrix degradation in human NPSCs. In an acidic microenvironment, ferroptosis is promoted due to enhanced NCOA4-mediated ferritinophagy in NPSCs. A mechanistic study demonstrated that RBX1-mediated ubiquitination modulated NCOA4 expression and the inhibition of RBX1 promoted ferroptosis through NCOA4-mediated ferritinophagy in the human NPSCs. Our in vivo study further illustrated that RBX1 overexpression ameliorated ferroptotic effects on IVDD progression by suppressing NCOA4-mediated ferritinophagy. Results demonstrated the modulating role of RBX1 in NCOA4-mediated ferritinophagy and NPSC ferroptosis, providing valuable insights into the potential application of endogenous stem cell–based IVD self-repair and self-regeneration for IVDD treatment.

†Lu-Ping Zhou, Liang Kang and Zhi-Gang Zhang contributed equally to the work and should be regarded as co-first authors.

*Correspondence:
Ren-Jie Zhang
zhangrenjie1089@126.com
Cai-Liang Shen
shencailiang@ahmu.edu.cn
Full list of author information is available at the end of the article

Introduction

Low back pain (LBP) is one of the primary causes of global disability [1]. Especially in adolescents and young adults, LBP is the most prevalent among musculoskeletal disorders worldwide, accounting for 76.4% of incident cases and 45.2% of prevalent cases [2]. Various potential factors are associated with LBP, and intervertebral disc (IVD) degeneration (IVDD) is one of its leading causes [3, 4]. IVDs are intricate and avascular fibrocartilaginous structures comprising the central highly hydrated gelatinous nucleus pulposus (NP), outer highly organized peripheral annulus fibrous (AF), and cartilaginous endplates (CEPs). IVDD is accompanied by the gradual loss of NP cells (NPCs), extensive shrinkage of NP, and remarkable increase in proinflammatory cytokines, thereby accelerating extracellular matrix (ECM) dehydration and catabolic cascades [5–7]. The loss of NPCs and subsequent decrease in ECM are some of the initiating events in IVDD and contribute to the deterioration of microenvironments, cellular functions, and biomechanical properties, finally resulting in discogenic LBP [5, 8].

NP-derived stem cells (NPSCs), which exist within an IVD, can self-renew and differentiate into NPCs, thus promoting the self-repair of NP tissues and self-regeneration of the ECM [9, 10]. Research on IVDD mechanisms is currently focused on NPCs for enhancing cell viability and reducing mortality [5, 11–13]. However, the intrinsic physiological mechanisms of NPSC-based therapy in IVDD remain poorly understood. NPSCs are a potentially valuable source of seed cells for cellular therapy and tissue engineering for IVD repair and regeneration [14–16]. Thus, understanding the molecular and pathological mechanisms underlying NPSCs can provide novel insights for improving IVDD treatment.

A degenerated IVD is surrounded by a harsh microenvironment characterized by acidosis, high osmolarity, limited nutrition, and accumulated proinflammatory factors [17–19]. An acidic pH of the microenvironment is one of the determining factors for the progression of IVDD, exacerbating ECM degradation, NPC dysfunctionality, and inflammation [20, 21]. An IVD, the largest avascular fibrocartilaginous tissue in the human body, primarily relies on anaerobic glycolysis for energy production, which is a process accompanied by lactate production [22]. Therefore, a healthy IVD typically maintains a slightly acidic microenvironment with a pH ranging from 7.2 to 7.0 [23]. However, when the permeability of CEP decreases during IVDD progression, the transport of nutrients and metabolites diminishes, resulting in a deteriorating microenvironment characterized by hypoxia, inflammation, and ischemia [17]. Tissue acidosis consequently occurs, decreasing the pH to 6.5 or lower [20, 24]. To date, the cellular and molecular regulatory changes underlying acidosis in NPSCs remain poorly documented.

The excessive accumulation of cellular iron, particularly ferrous iron, can lead to lipid peroxidation through a Fenton reaction, thereby activating ferroptosis, which is a form of programmed cell death dependent on iron [25, 26]. Disturbed iron homeostasis results in excessive reactive oxygen species (ROS) generation, mitochondrial dysfunction, oxidative stress, and DNA damage, ultimately destroying cell structure and function [27]. Cellular iron overload and resultant ferroptosis are implicated in many degenerative diseases, including Parkinson's disease [28], Alzheimer's disease [29], amyotrophic lateral sclerosis [30], and sarcopenia [31]. Many studies have reported the regulatory mechanism of ferroptosis in IVDD; however, these studies mainly simulated a degenerative microenvironment of the IVD by inducing oxidative stress by using tert-butyl hydroperoxide (TBHP) [32–34], inflammatory conditions by using IL-6 [35] and IL-1β [36], or iron overload conditions by using ferric ammonium citrate (FAC) [37]. Whether acidic conditions can induce ferroptosis is still unknown. In addition, the specific biological activity and underlying pathological mechanisms of NPSCs during ferroptosis are yet to be determined.

Ferritin is the primary iron storage protein, storing approximately 70%–80% of newly imported iron [38]. Nuclear receptor coactivator 4 (NCOA4) is a selective cargo receptor mediating the autophagic degradation of ferritin in a process termed "ferritinophagy." [39]. Ferritinophagy regulates iron homeostasis, and the excessive degradation of ferritin through ferritinophagy can lead to the accumulation of iron and trigger ferroptosis [40]. Given that NCOA4 is widely expressed in mammalian cells, ferritinophagy has been observed in many pathological processes. However, the role of NCOA4-mediated ferritinophagy in the pathogenesis of NPSCs during IVDD progression remains poorly understood.

In this study, we investigated whether an acidic conditions can induce ferroptosis in NPSCs and aggregate IVDD through ferroptosis and examined the role of NCOA4-mediated ferritinophagy in NPSC ferroptosis and IVDD pathogenesis. We further explored the regulatory mechanisms underlying the expression of NCOA4 and investigated whether the knockdown of ring-box 1 (RBX1), the E3 ubiquitin ligase targeting NCOA4, promotes the ferroptosis and IVDD progression by upregulating NCOA4-mediated ferritinophagy.

Methods

Clinical study

The protocol of this clinical study was reviewed and approved by the ethics committee of our hospital, and

informed consent forms were obtained from all the included patients.

A total of 204 patients diagnosed with IVD herniation were recruited from April 2023 to August 2023. The inclusion and exclusion criteria are shown in Supplementary Text 1. Peripheral blood samples were collected for the measurement of iron metabolism biomarkers, including serum ferritin, transferrin, serum iron, unsaturated iron-binding capacity (UIBC), and total iron-binding capacity (TIBC). The degree of IVD degeneration was blindly evaluated by two experienced spinal surgeons, who performed preoperative T2-weighted magnetic resonance imaging (MRI) and used the Pfirrmann grading system [41]. Any disagreement was settled by a third senior surgeon. Information regarding the demographic and health-related factor assessment and reagents used in the clinical study is displayed in Supplementary Text 1. All blood samples were handled by a researcher blinded to the patients, and a Hitachi Automatic Analyzer 3100 (Hitachi, Japan) was used for sample analysis.

Human NP samples

The method for collecting human NP tissues was approved by the ethics committee of our hospital. Prior to the acquisition of tissues, informed consent was obtained from all participants or their legal guardians. Human NP tissues were obtained from twenty patients (10 males and 10 females) who underwent spinal surgery for degenerative disc disease. The degree of disc degeneration was assessed through preoperative T2-weighted MRI according to the Pfirrmann grading system. The samples were promptly sectioned for subsequent experiments, including cell isolation and culture, quantitative real-time PCR (qRT-PCR) assay, and protein analysis.

Isolation and culture of human NPSCs

Human NP tissues isolated from peripheral annulus fibrous tissues were washed three times with sterile phosphate-buffered saline (PBS), carefully cut into ~0.5 mm × 0.5 mm × 0.5 mm pieces with sterile ophthalmic scissors, and enzymatically digested with 0.2% type II collagenase at 37 °C for 4 h. After the tissue suspension was centrifuged at 1000×*g* for 5 min, the collected cells were resuspended and cultured in low-glucose Dulbecco's modified Eagle's medium supplemented with 10% fetal bovine serum and 1% penicillin–streptomycin solution and placed in a humidified incubator at 37 °C with 5% CO_2. The culture medium was replaced twice a week, and the cells at the second or third passage were prepared for the in vitro experiments.

Cell viability assays

NPSC viability was evaluated using the cell counting kit-8 (CCK-8, Biosharp, BS350A) in accordance with the manufacturer's instructions. NPSCs were seeded in 96-well plates at a density of 5×10^3 cells/well and then treated with different interventions. Cell viability was assessed at various time points, and the culture media were replaced with 100 µl of standard medium supplemented with 10 µl of CCK-8 solution. After 4 h of incubation at 37 °C in the absence of light, the optical density (OD) was measured by detecting the absorbance at 450 nm with a multimode plate reader (PE EnSpire, USA).

Western blot analysis

The cells were lysed using a RIPA assay kit (Beyotime, P0013) on ice and centrifuged, and proteins were collected. Protein concentration was measured using a BCA assay kit (Beyotime, P0012S). Equal amounts of total protein (20 µg) mixed with loading buffer (Beyotime, P0015) were boiled at 100 °C for 10 min. The proteins in each sample were separated by electrophoresis through SDS-PAGE and then transferred to a PVDF membrane (Millipore, United States). The membranes were blocked with 5% skim milk in Tris-buffered saline with Tween-20 (TBST) for 2 h and then incubated with the following primary antibodies overnight at 4 °C: NCOA4 (HUABIO, ER62707; 1:1000), RBX1 (HUABIO, ER1802-9; 1:500), MDM2 (HUABIO, ER1902-14; 1:1000), FTH1 (HUABIO, ET1610-78; 1:500), GPX4 (HUABIO, ET1706-45; 1:1000), SLC7A11 (Immunoway, YT8130; 1:1000), MMP3 (HUABIO, ER1706-77; 1:500), ADAMTS5 (Immunoway, YN2121; 1:1000), and GAPDH (HUABIO, ET1601-4; 1:10,000). The membranes were washed with TBST three times and then incubated with the corresponding species-specific secondary antibodies for 1 h at room temperature. GAPDH was used as the internal control. The intensities of the membrane signals were measured using an AL600RGB gel imaging system (GE, USA).

Detection of intracellular ROS

Human NPSCs were seeded in 12-well plates, attached to slides, and subjected to different interventions. After treatment, the cells were washed with PBS, exposed to 10 µM DCFH-DA fluorescent probe (Beyotime, S0033S) in the dark for 20 min at 37 °C, washed again, and finally observed using a fluorescence microscope (Leica DM6 B, Germany).

Immunofluorescence staining

NPSCs cultured in six-well plates and attached to slides were fixed with 4% paraformaldehyde for 15 min, permeabilized for 30 min using 0.2% Triton X-100 (Biosharp,

BL935A), and incubated. The cells were then washed with PBS and blocked with 5% bovine serum albumin dissolved in PBS for 2 h at 37 °C. Primary antibodies, namely, GPX4 (HUABIO, ET1706-45, rabbit mAb; 1:100), FTH1 (Novus, MAB9354, mouse mAb; 1:100), and NCOA4 (Proteintech, 10968-1-AP, rabbit pAb; 1:100), and the cells were then incubated with the respective secondary antibodies. Subsequently, the cells were washed with PBS three times and incubated with DAPI (Beyotime, C1006) for 5 min. Images were scanned using a fluorescence microscope (Leica DM6 B, Germany).

Mitochondrial membrane potential (MMP, Δψm) detection

After the interventions, a prepared JC-1 (Beyotime, C2003S) reaction solution was introduced to the cells and incubated at 37 °C for 30 min. Subsequently, the cells were washed with a configured JC-1 buffer and observed under a fluorescence microscope (Leica DM6 B, Germany).

Iron assay

Intracellular iron levels were measured with a cell total iron colorimetric assay kit (Elabscience, E-BC-K880-M) according to the manufacturer's instructions. The cells were lysed with iron assay buffer (Reagent 1) on ice for 10 min and centrifuged at 15,000×*g* for 10 min. The supernatant was carefully preserved and incubated with chromogenic solution (Reagent 2) at 45 °C for 1 h. Finally, the absorbance was promptly measured at 593 nm emission wavelength with the multimode plate reader (PE EnSpire, USA), and iron concentrations were determined using the standard calibration curve method.

Measurement of glutathione (GSH) and malonaldehyde (MDA) levels

The levels of glutathione (GSH) and malonaldehyde (MDA) were analyzed using a GSH colorimetric assay kit (Elabscience, E-BC-K030-M) and MDA Assay Kit (Beyotime, S0131S) in accordance with the manufacturer's instructions. The MDA and GSH levels were measured against the standard calibration curves based on absorbances at 532 and 405 nm with the multimode plate reader (PE EnSpire, USA).

qRT-PCR assay

RNA was extracted using a total RNA extraction kit (Omega Biotek, R6834-01) and reversely transcribed into cDNA with a NovoScript Plus all-in-one first-strand cDNA synthesis SuperMix (Novoprotein, E047-01B) in accordance with the manufacturer's instructions. Quantitative real-time PCR was performed using NovoStart®SYBR qPCR SuperMix Plus (Novoprotein, E096-01A). The primer sequences are listed in Supplementary Table 2. Gene expression was calculated using the $2^{-\triangle\triangle Ct}$ method.

Small interfering RNA (siRNA), plasmids, and transfection

Small interfering RNAs (siRNAs) specifically targeting *NCOA4*, *RBX1*, and *MDM2* and control-siRNAs were synthesized by RiboBio Co., Ltd. (Guangzhou, China). The siRNA sequences are shown in Supplementary Table 1. After reaching 60%–70% confluence, human NPSCs were transfected with siRNAs with a riboFECTTM CP transfection kit (R10035.4) in accordance with the manufacturer's instructions. The modified siRNA used in the animal experiments was purified using the riboFECTTM CP transfection kit (R10035.4) before injection. The plasmid for *NCOA4* overexpression and negative control plasmid were synthesized using a riboFECTTM CP transfection kit (R10035.4). After reaching 60%–70% confluence, the human NPSCs were infected with purified plasmid with Lipofectamine 2000 (Invitrogen, 11668019) according to the manufacture's instruction.

Co-immunoprecipitation (Co-IP) assay

Human NPSCs were lysed using an IP lysis buffer, and the supernatant was obtained after centrifugation at 12,000×*g* for 15 min. The lysates were precleared by adding rProtein A/G MagPoly beads (ACE Biotechnology, AM001-02) at 4 °C for 30 min. For the generation of immune complexes with NCOA4 protein (or FTH1 protein/RBX1 protein), the lysates were incubated with anti-NCOA4 antibody (or Anti-FTH1 antibody/Anti-RBX1 antibody) overnight at 4 °C. Subsequently, rProtein A/G MagPoly beads were added to the lysates for 2 h at 4 °C, followed by washing with lysis buffer five times. Finally, the bound proteins were eluted using a loading buffer and denatured through boiling. Equivalent protein samples were employed for Western blot analysis.

Protein degradation assay

We treated human NPSCs with MG132 (MCE, HY-13259) to suppress proteasome-mediated protein degradation and investigate whether RBX1 destabilizes NCOA4 protein.

Overexpression of NCOA4 with an adeno-associated virus in vivo

An adeno-associated virus containing *Rbx1* (AAV-*Rbx1*) or *Ncoa4* (AAV-*Ncoa4*) was injected into the discs of 3-month-old rats. Rats that did not require AAV- *Rbx1* or AAV-*Ncoa4* injection were all treated with negative control (AAV-GFP) in the same period.

Animal experiment

The animal experiment was approved by the animal care committee of the medical university. Fifty Sprague–Dawley rats (3 months old, weighing 200–300 g) for the IVDD model were purchased from the animal center of the medical university. The rat models of IVDD were established according to previous methods [42, 43]. The rats were randomly assigned to five groups with 10 rats each: control (no IVD puncture), IVDD (subjected to needle puncture, Control-siRNA, and AAV-GFP), IVDD + *Ncoa4*-siRNA group (subjected to needle puncture, *Ncoa4*-siRNA, and AAV-GFP), IVDD + AAV-*Rbx1* group (subjected to needle puncture, Control-siRNA, and AAV-*Rbx1*), and IVDD + AAV-*Rbx1* + AAV-*Ncoa4* group (subjected to needle puncture, Control-siRNA, AAV- *Rbx1*, and AAV-*Ncoa4*). They were housed under highly controlled living conditions. An operator blinded to the group assignment independently conducted the experiment. Sodium pentobarbital (30 mg/kg) was used to anesthetize the rats. Needles (29-G) were used in performing needle-to-percutaneous disc puncture on the experimental disc level (Co 7/8) located through digital palpation. The syringe needle perpendicular to the tail was inserted into the disc, penetrating a depth of at least 5 mm within the disc. The needle was then rotated 360° and kept within the disc for 60 s to induce degenerative effects. Afterward, *Ncoa4*-siRNA, Control-siRNA, AAV-*Rbx1*, AAV-*Ncoa4*, and AAV-GFP were injected. siRNAs were administered at 5-day intervals with a small 31-G needle to minimize injury to AF. AAV-*Rbx1*, AAV-*Ncoa4*, and AAV-GFP were only administered at the first injection. All animals were provided with unrestrained weight bearing and unrestricted activity. Four weeks after surgery, all the rats were anesthetized and underwent MRI examination. The degree of IVDD was evaluated using the Pfirrmann grading system. Finally, the rats were euthanized, and their IVDs were harvested for histological analysis (five rats per group), and MDA and GSH levels were analyzed (five rats per group).

Western blot, immunohistochemistry (IHC) and immunostaining assays in NP tissues and animal models

For Western blot analysis, frozen tissues were homogenized, and total protein was extracted. The subsequent procedure was conducted as previously described. For histological analysis, the discs were washed with PBS and then fixed in a 4% formaldehyde solution with a pH of 7.4 for 12 h. Decalcification was performed using 10% formic acid solution. The discs were dehydrated with a graded series of ethanol, embedded in paraffin, and sectioned at a thickness of 4 μm. Finally, the sections were deparaffinized, rehydrated, and stained with hematoxylin and eosin (H&E), Alcian blue, and Safranin-*O*. For tissue immunohistochemistry (IHC) and immunofluorescence, the prepared slides were incubated with primary GPX4 (HUABIO, ET1706-45, rabbit mAb; 1:100) and TEK (Proteintech, 19157-1-AP, rabbit mAb; 1:300). The sections were then incubated with corresponding secondary antibodies and counterstained with DAPI (Beyotime, C1006).

Statistical analysis

Continuous variables were presented as mean ± SD, and categorical variables were reported as absolute (no.) and relative frequencies (%). For clinical study, data were analyzed using SPSS software (version 26.0, IBM), Medcalc software (version 19.5.6, Medcalc Software Ltd.), and Prism statistical software (version 9.5.1, GraphPad). Data from the in vivo and in vitro experimental groups were compared using student's *t*-test for two groups and one-way or two-way analysis of variance for multiple groups with Prism statistical software (version 9.5.1, GraphPad). A *P*-value less than 0.05 was deemed statistically significant. Other methods of statistical analysis are listed in Supplementary Text 2. Additionally supplementary materials are displayed in Supplementary Text 3.

Results

Serum ferritin is negatively correlated with IVDD severity

To better understand the association between iron metabolism and IVDD progression, we prospectively recruited 204 patients with different levels of IVDD severity who met the indications of lumber spine surgery (Supplementary Tables 3 and 4) and collected the peripheral blood from these patients before the surgery. To analyze the correlation between iron metabolic biomarkers (an indicator of iron metabolism) in peripheral blood and IVDD severity, we examined the levels of serum ferritin, transferrin, serum iron, UIBC, and TIBC in the included patients. The cumulative Pfirrmann grades of the five lumber segments of IVD (namely, the discs of L1/2, L2/3, L3/4, L4/5, and L5/S1) were calculated and finally characterized by a range of cumulative grade number from 9 to 22 for each patient. The correlation analyses showed that levels of serum ferritin, serum iron, and UIBC were significantly associated with the cumulative Pfirrmann grades, respectively (Fig. 1A–C, Supplementary Fig. 1A and 1B, and Supplementary Table 5).

Given that iron metabolism exhibits gender differences and ferritin levels in males are typically two or three times those in females [44], we analyzed the correlation of iron metabolic biomarkers and cumulative Pfirrmann grades in males and females. We found that only the levels of serum ferritin, rather than serum iron and UIBC levels, was significantly associated with cumulative Pfirrmann grades in females ($r = -0.5479$, $P < 0.0001$) and

males ($r = -0.3548$, $P = 0.0001$; Fig. 1D–I, Supplementary Fig. 1C–F, and Supplementary Table 6). Additionally, logistic regression analysis indicated that reduction in serum ferritin levels independent of other factors, including the age and body mass index, was associated with severe IVDD in both genders (Supplementary Table 7). To further support this notion, we performed Mann–Whitney U tests and identified a cutoff value of cumulative Pfirrmann grades, using serum ferritin concentration to distinguish between IVDs with mild and severe degeneration. The Z value of Mann–Whitney U test adjusted by LOWESS for serum ferritin is shown in Supplementary Tables 8 and 9. Finally, the LOWESS curves showed that the cutoff value of cumulative grade to discriminate the severity of disc degeneration was 16 in both males and females (Fig. 1J and K). The ROC curves revealed that ferritin was a more effective predictor for high cumulative Pfirrmann grades than the other indicators of iron metabolism in both genders (Fig. 1L and M; and Supplementary Table 10). Moreover, the concentration of serum ferritin, instead of iron and UIBC concentrations, in patients in the high degeneration score group (cumulative Pfirrmann grades ≥ 16) significantly decreased compared with that in patients in the low degeneration score group (cumulative Pfirrmann grades < 16; Fig. 1N and O, Supplementary Fig. 1G–J, and Supplementary Table 11). Taken together, these results revealed that a low concentration of ferritin indicates severe IVDD.

Ferroptosis progressively increases in human NP tissues as IVDD advances

Given that peripheral ferritin was closely associated with IVDD severity, we further investigated the role of ferroptosis in human local NP tissues during IVDD progression. According to the Pfirrmann classification based on the preoperative MRI scans [41], we collected four discs with mild degeneration and four with severe degeneration from eight patients who received spinal surgery (Fig. 2A). The Pfirrmann classifications of these NP tissues were verified according to histological characteristics. The severely degenerated discs indicated atrophic volume and decreased elasticity compared with mildly degenerated discs. (Fig. 2B). We then investigated the expression levels of ferroptosis markers, including GPX4 and SLC7A11, and ECM degradation markers, including ADAMTS5 and MMP3, through Western blot analysis. As presented in Fig. 2C–D, the global levels of GPX4 and SLC7A11 in the severe-IVDD group were significantly lower than those in the mild-IVDD group. Meanwhile, the expression levels of ADAMTS5 and MMP3 in the severe-IVDD group were significantly higher than those in the mild-IVDD group. Additionally, according to IHC assay, we found low GPX4 levels in remarkably degenerated NP tissues (Fig. 2E and F). Consistently, the mRNA level of *GPX4* significantly decreased in the severe-IVDD group, compared with that in the mild-IVDD group (Fig. 2G). We also measured the content of other ferroptosis markers, including GSH (a negative indicator of ferroptosis [45]) and MDA (a positive indicator of ferroptosis [46]), in the mildly and severely degenerated IVDD tissues. Compared with the mild-IVDD group, the severe-IVDD group showed reduced GSH levels and increased MDA (Fig. 2H and I). Overall, these results indicated that ferroptosis promote IVDD progression.

Acidic conditions induce ferroptosis-associated cell viability decline, ROS accumulation, and ECM degradation in human NPSCs

The cells in a degenerated IVD have unusual acidic microenvironments, which lead to low pH levels [47]. Given that stem cell death is concomitant with the progression of ferroptosis and IVDD, we investigated the role of ferroptosis in NPSCs under an acidic condition. We first isolated the cells from NP tissues and identified the characteristics of the isolated cells. These cells at the fourth passage still possessed adipogenic, osteogenic, and chondrogenic differentiation potency, identified as the NPSCs. (Supplementary Fig. 2A) We used the second

(See figure on next page.)

Fig. 1 The levels of serum ferritin in male and female patients were negatively correlated with IVDD severity. **A**–**C** Correlation analyses between iron metabolism indicators and cumulative Pfirrmann grades. The results showed that levels of serum ferritin, serum iron, and UIBC were significantly associated with the cumulative Pfirrmann grades, respectively. **D**–**F** Correlation analyses between iron metabolism indicators and cumulative Pfirrmann grades in female blood samples. The results showed that only the level of serum ferritin, rather than the serum iron and UIBC, was significantly associated with cumulative Pfirrmann grades. **G**–**I** Correlation analyses between iron metabolism indicators and cumulative Pfirrmann grades in male blood samples. The results showed that only the level of serum ferritin, rather than the serum iron and UIBC, was significantly associated with cumulative Pfirrmann grades. **J**–**K** LOWESS curves using serum ferritin levels were applied to ascertain the optimal cut-off value for distinguishing the mild- and severe-degenerated IVDs in female and male blood samples. **L**–**M** Receiver operating characteristic (ROC) curves to determine the predictive performance of serum ferritin, serum iron, and UIBC for low- and high- cumulative Pfirrmann grades. **N** The levels of serum ferritin in high cumulative Pfirrmann grades compared to those in low cumulative Pfirrmann grades for samples from female cohorts. **O** The levels of serum ferritin in high cumulative Pfirrmann grades compared to those in low cumulative Pfirrmann grades for samples from male cohorts. A *P*-value less than 0.05 was deemed to be statistically significant. (***$P < 0.001$; ****$P < 0.0001$)

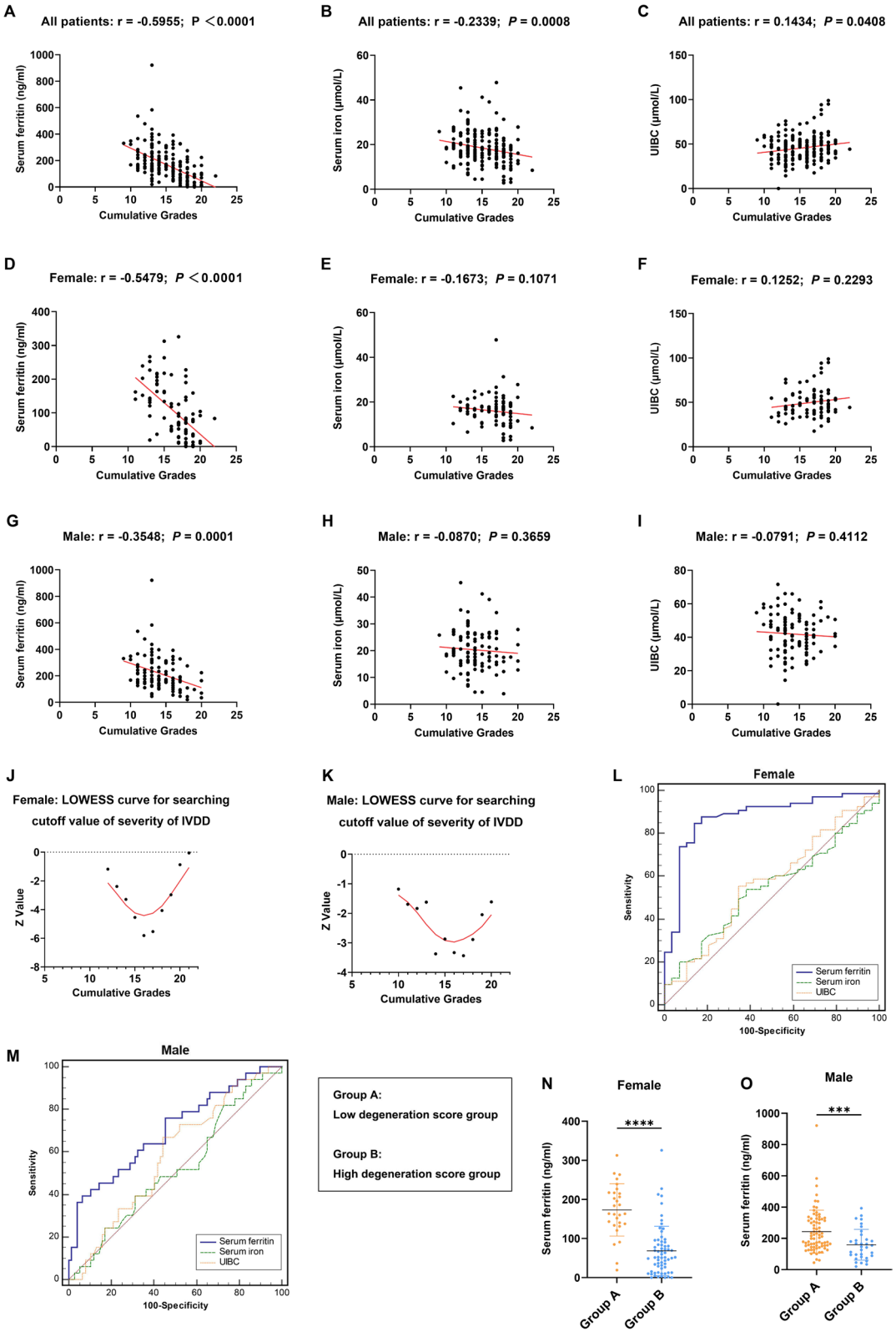

Fig. 1 (See legend on previous page.)

or third generation of cells for most of the experiments. Then we treated the NPSCs with hydrochloric acid at different concentrations to obtain condition medium with different pH (7.1, 6.8, 6.5, and 6.2) for 12, 24, or 48 h [48]. CCK-8 assay revealed that the viability of the NPSCs cultured with a pH at 6.8 significantly decreased at 48 h, rather than at 12 and 24 h, compared with the viability under a physiological acidic condition (pH = 7.1) [49]. Additionally, the acidic condition with a pH of 6.5 significantly impaired the growth of NPSCs at 24 and 48 h. The acidic condition with a pH of 6.2 significantly impaired the growth of NPSCs over a period of 12, 24, or 48 h (Fig. 3A and Supplementary Table 12). Consistently, an acidic condition after 24 h of culture significantly promoted the expression of MMP3 and ADAMTS5 in the NPSCs, suggesting an increase in the level of ECM degradation (Fig. 3B and C).

We next examined changes in ferroptosis-associated proteins under acidic conditions. The expression levels of GPX4 and SLC7A11 significantly decreased under acidic conditions compared with those under normal condition after 24 h of treatment, suggesting that acidic condition in culture would lead to ferroptosis of NPSCs (Fig. 3D and E). To further investigate the correlation between ferroptosis and abnormal acidic microenvironments in NPSCs, we applied ferrostatin-1 (Fer-1), an inhibitor of ferroptosis, to block ferroptosis in NPSCs in an acidic environment. Immunofluorescence staining of GPX4 showed that the relative fluorescence intensity significantly increased after Fer-1 treatment in an acidic condition compared with the relative fluorescence intensities after acidic treatment (Fig. 3F and G). As expected, Fer-1 consumption significantly increased the expression levels of GPX4 and SLC7A11 (Fig. 3H, I, J) and alleviated ECM degradation (Fig. 3H, K, L) in the NPSCs.

Ferroptosis is accompanied by mitochondrial stress including the higher level of intracellular ROS and decreased mitochondrial membrane potential. Immunofluorescence revealed that Fer-1 blocked ROS accumulation induced by an acidic condition (Fig. 3M, N). In addition, Fer-1 reversed the decrease in MMP ($\Delta\psi m$) levels after an acidic treatment (Fig. 3O, P). Moreover, increased intracellular MDA and iron levels in acidic-induced NPSCs were blocked by Fer-1 (Fig. 3Q, R). Overall, these results suggested that an acidic condition promotes ferroptosis in NPSCs and induces cell viability decline, ROS accumulation, and ECM degradation through ferroptosis in human NPSCs.

NCOA4-mediated ferritinophagy participates in acidic-induced ferroptosis in human NPSCs

To determine the mechanism underlying iron accumulation and associated ferroptosis under acidic conditions in NPSCs, we conducted Western blot analysis to investigate the levels of transferrin receptor (TFR) and divalent metal transporter 1 (DMT1) associated with the uptake of ferroportin 1 (FPN1), which is involved in iron transport, and NCOA4, which is a selective cargo receptor regulating the autophagic degradation of ferritin. No significant differences in the expression levels of TFR and DMT1 were observed when the pH levels decreased from 7.1 to 6.2 for 24 h after acidic treatment (Fig. 4A and Supplementary Fig. 3A and B). The levels of FPN1 significantly increased at pH of 6.8, but no significant difference was observed between FPN1 levels at pH of 6.5 or 6.2 and those under a physiological acidic condition (Fig. 4A and Supplementary Fig. 3C). Notably, the expression of NCOA4 significantly increased at pH 6.8–6.2, compared with that under a normal condition (Fig. 4A and B). Therefore, the progression of ferroptosis under acidic conditions in human NPSCs might be triggered by the elevated expression of NCOA4. To clarify the regulatory role of NCOA4 on the progression of ferroptosis, we used the STRING database for target prediction (Fig. 4C) [50]. FTH1 had the highest confidence on the functional link and interaction with NCOA4 (combined score: 0.999). FTH1, the H subtype of ferritin, mainly facilitated the storage of intracellular iron, whose proteolytic degradation can contribute to the rapid release of free iron and subsequent Fenton reaction [26]. Western blot analysis indicated that the level of FTH1 protein significantly decreased after acidic intervention in the NPSCs (Fig. 4D and E). To further identify the interaction between NCOA4 and FTH1, we performed a Co-IP experiment, which demonstrated that NCOA4 directly targeted FTH1 (Fig. 4F). Therefore, we speculated that

(See figure on next page.)

Fig. 2 Ferroptosis progressively increased in human NP tissues as IVDD advanced. **A** Representative MRI images of human NP tissues with different degrees of degeneration. Four discs samples with mild degeneration and four with severe degeneration from eight patients were collected. **B** H/E and Alcian blue staining of human NP samples in NP tissues from Pfirrmann grades II and V. Scale bar: 25 μm. **C**, **D** Representative western blot images of ferroptosis-associated proteins GPX4, FTH1, and SLC7A11, and ECM degradation-associated proteins MMP3 and ADAMTS5 in NP tissues from Mild- and Severe- IVDD groups. The relative band densities were quantified. **E**, **F** IHC staining of GPX4 in human nucleus pulposus sections. Scale bar: 25 μm. Quantitative analysis was shown as percentage of $GPX4^+$ cell in NP tissues. **G** The relative mRNA levels of *GPX4* in NP tissues from Mild- and Severe-IVDD groups. **H** Relative GSH levels in NP tissues from Mild- and Severe-IVDD groups. **I** Quantification of MDA contents in NP tissues from Mild- and Severe-IVDD groups. (*$P < 0.05$; **$P < 0.01$; ***$P < 0.001$; ****$P < 0.0001$)

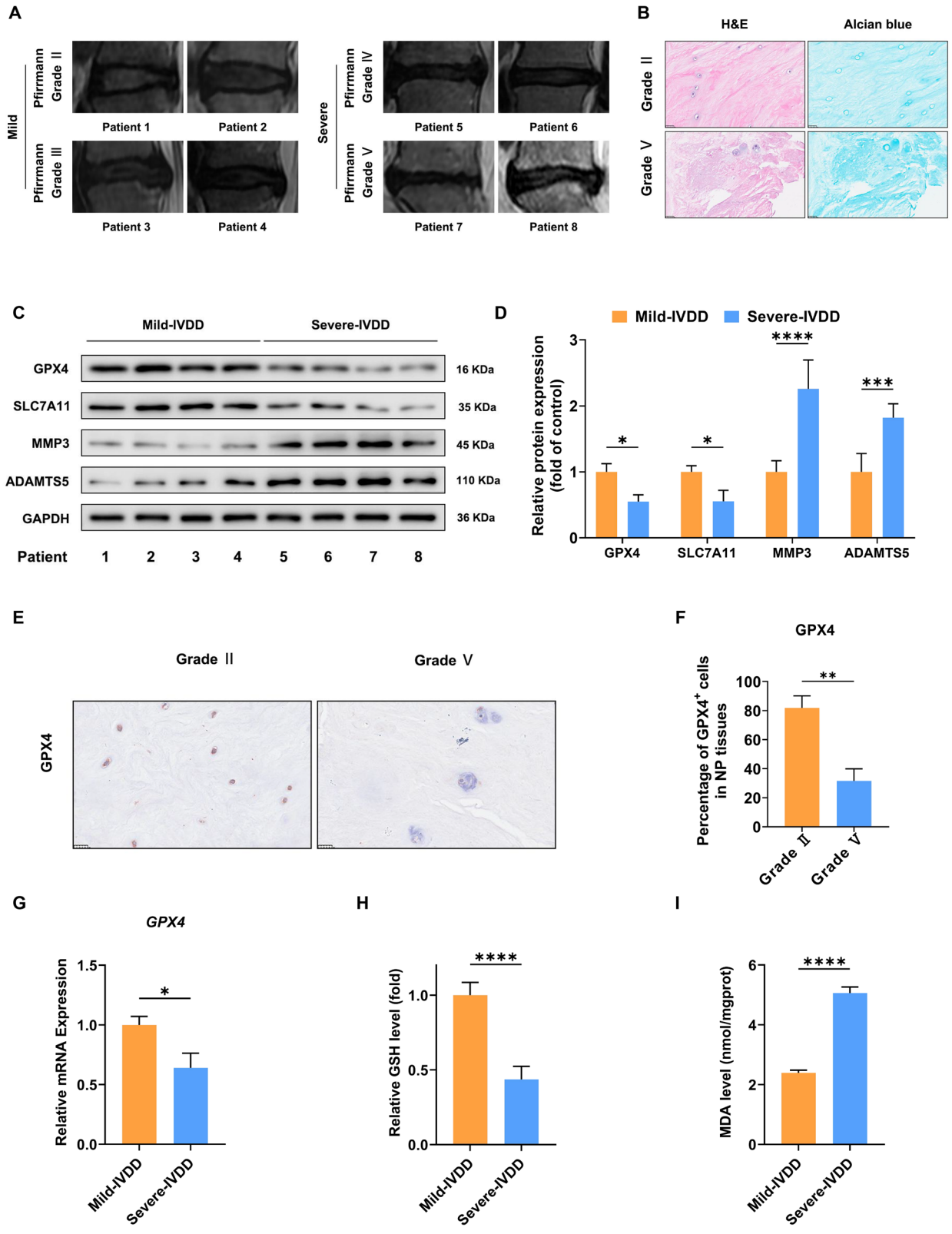

Fig. 2 (See legend on previous page.)

the NCOA4-mediated degradation of ferritin (also called ferritinophagy) plays an important role in the molecular mechanism of acidic-dependent ferroptosis.

Given that ferritinophagy is a selective form of autophagy, the role of autophagy in the degradation of ferritin was explored using Western blot analysis. As shown in Fig. 4G and Supplementary Fig. 3D, the protein level of FTH1 was significantly rescued after the NPSCs were treated with 3-methyladenine (3-MA) or chloroquine (CQ) in an acidic microenvironment. Meanwhile, a significant increase was observed in the levels of GPX4 and SLC7A11 proteins, which are both markers of ferroptosis (Fig. 4G and Supplementary Fig. 3E and F). The levels of ADAMTS5 and MMP3 proteins, which are ECM degradation markers, decreased considerably upon the administration of 3-MA or CQ compared with those in the untreated NPSCs (Fig. 4G and Supplementary Fig. 3G and H). Thus, the degradation of ferritin can be blocked through autophagic inhibition, and the suppression of ferritinophagy can alleviate ferroptosis in NPSCs.

Stable *NCOA4*-deficent NPSCs were generated to further determine the biological effects of NCOA4 in ferritinophagy and ferroptosis. As shown in Supplementary Fig. 3I and J, *NCOA4*-siRNA1 was utilized in subsequent research because it has higher knockdown efficiency than *NCOA4*-siRNA2 and *NCOA4*-siRNA3. Compared with those in the control group (without transfection of *NCOA4*-siRNA1), ferroptotic process and ECM degradation were significantly inhibited by NCOA4 knockdown, as evidenced by the increased expression of ferroptosis markers and FTH1, GPX4, and SLC7A11 proteins and the reduced expression of MMP3 and ADAMTS5 proteins after *NCOA4* knockdown in acidic treatment (Fig. 4H and Supplementary Fig. 3K–O). The immunofluorescence staining of FTH1 and NCOA4 indicated that the number of red punctae decreased in the NPSCs stimulated by an acidic condition but increased in the *NCOA4*-knockdown NPSCs after acidic treatment relative to the number of red punctae in the control group (Fig. 4I). Immunofluorescence staining of GPX4 confirmed that the relative fluorescence intensity significantly increased in the *NCOA4*-siRNA group compared with the control-siRNA group under acidic treatment (Fig. 4J and Supplementary Fig. 3P). Immunofluorescence assay also revealed that NCOA4 knockdown significantly reduced ROS accumulation under an acidic condition in culture (Supplementary Fig. 3Q and R). Additionally, we found that the increased intracellular iron levels and MDA in acid-treated NPSCs were substantially rescued by NCOA4 knockdown (Fig. 4K and L). In summary, NCOA4 can mediate ferritinophagy and associated ferroptosis in NPSCs in an acidic microenvironment.

RBX1-mediated ubiquitination modulates NCOA4 expression

Given that the levels of NCOA4 proteins were progressively elevated under conditions with decreasing pH gradient, we speculated that the elevated levels of NCOA4 proteins in an acidic condition are due to the increased mRNA synthesis of *NCOA4*. We first performed qRT-PCR assay to examine the mRNA levels of *NCOA4* in human NPSCs with or without acidic treatment. However, no significant difference in *NCOA4* mRNA level was found between physiological (pH = 7.1) and acidic microenvironments (pH = 6.5), suggesting another molecular mechanism is involved in NCOA4 proteins expression (Fig. 5A).

The ubiquitin–proteasome system post-translationally controls the degradation of endogenous proteins by regulating the ubiquitination of target proteins. We hypothesized that high expression of NCOA4 is caused by low levels of ubiquitination. To clarify the regulatory mechanism for NCOA4 degradation, we used the online tool UbiBrowser to predict the potential E3 ligases targeting NCOA4 as the substrate [51, 52]. Finally, 13 predicted proteins that potentially interact

(See figure on next page.)

Fig. 3 Acidic condition induced ferroptosis-associated cell viability decline, ROS accumulation, and ECM degradation in human NPSCs. **A** Cell viability was detected by an CCK-8 assay in different groups. **B**, **C** Representative western blot images of ECM degradation-associated proteins MMP3 and ADAMTS5 in the acidic-treated NPSCs. The relative band densities were quantified. Western blot analysis showing the expression levels of MMP3 and ADAMTS5 as the pH levels decreased from 7.1 to 6.2. **D**, **E** Representative western blot images of ferroptosis-associated proteins GPX4 and SLC7A11 in the acidic-treated NPSCs. The relative band densities were quantified. Western blot analysis showing the expression levels of ferroptosis-associated proteins GPX4 and SLC7A11 as the pH levels decreased from 7.1 to 6.2. **F**, **G** After treatment with acidic conditions and acidic conditions + Fer-1 for 24 h, NPSCs were labeled with anti-GPX4 antibodies, and representative fluorescence images are shown. Nuclei were stained with DAPI. Scale bar: 50 μm. Quantitative analysis of GPX4 was shown as relative fluoresence intensity. **H**–**L** Representative western blot images of ferroptosis-associated proteins GPX4 and SLC7A11, and ECM degradation-associated proteins MMP3 and ADAMTS5 after NPSCs treated with acidic conditions and acidic conditions + Fer-1 for 24 h. The relative band densities were quantified. **M**, **N** Representative fluorescence microscopy photomicrographs of intracellular ROS in NPSCs. Scale bar: 50 μm. Quantitative analysis of intracellular ROS was shown as relative fluoresence intensity. **O**, **P** JC-1 staining for mitochondrial membrane potential in NPSCs. Scale bar: 200 μm. Quantitative analysis of mitochondrial membrane potential was shown as the ratio of monomer/aggregate. **Q** Quantification of MDA contents in NPSCs. **R** Total iron levels in NPSCs. A *P*-value less than 0.05 was deemed to be statistically significant. (*$P < 0.05$; **$P < 0.01$; ***$P < 0.001$; ****$P < 0.0001$; ns, not significant)

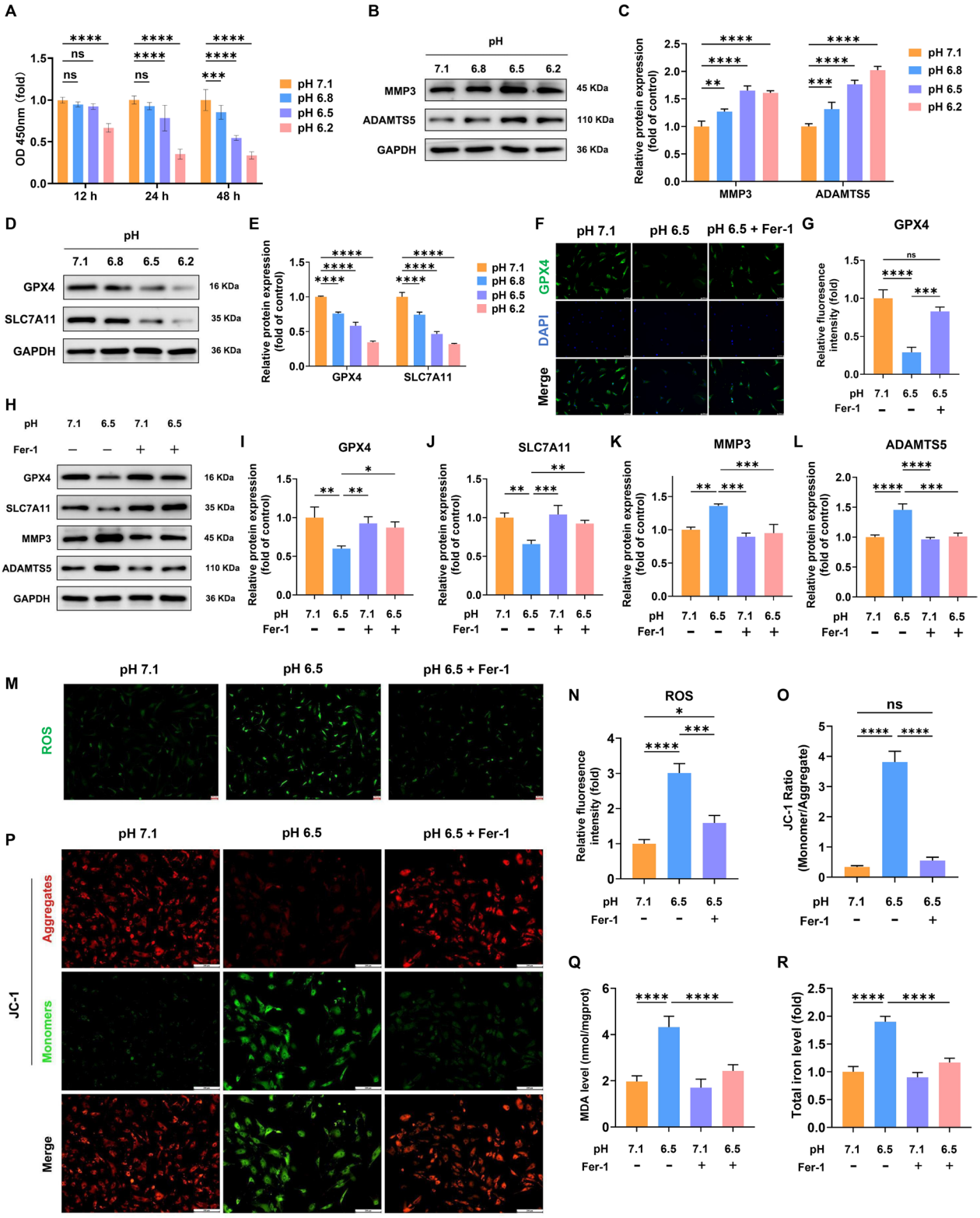

Fig. 3 (See legend on previous page.)

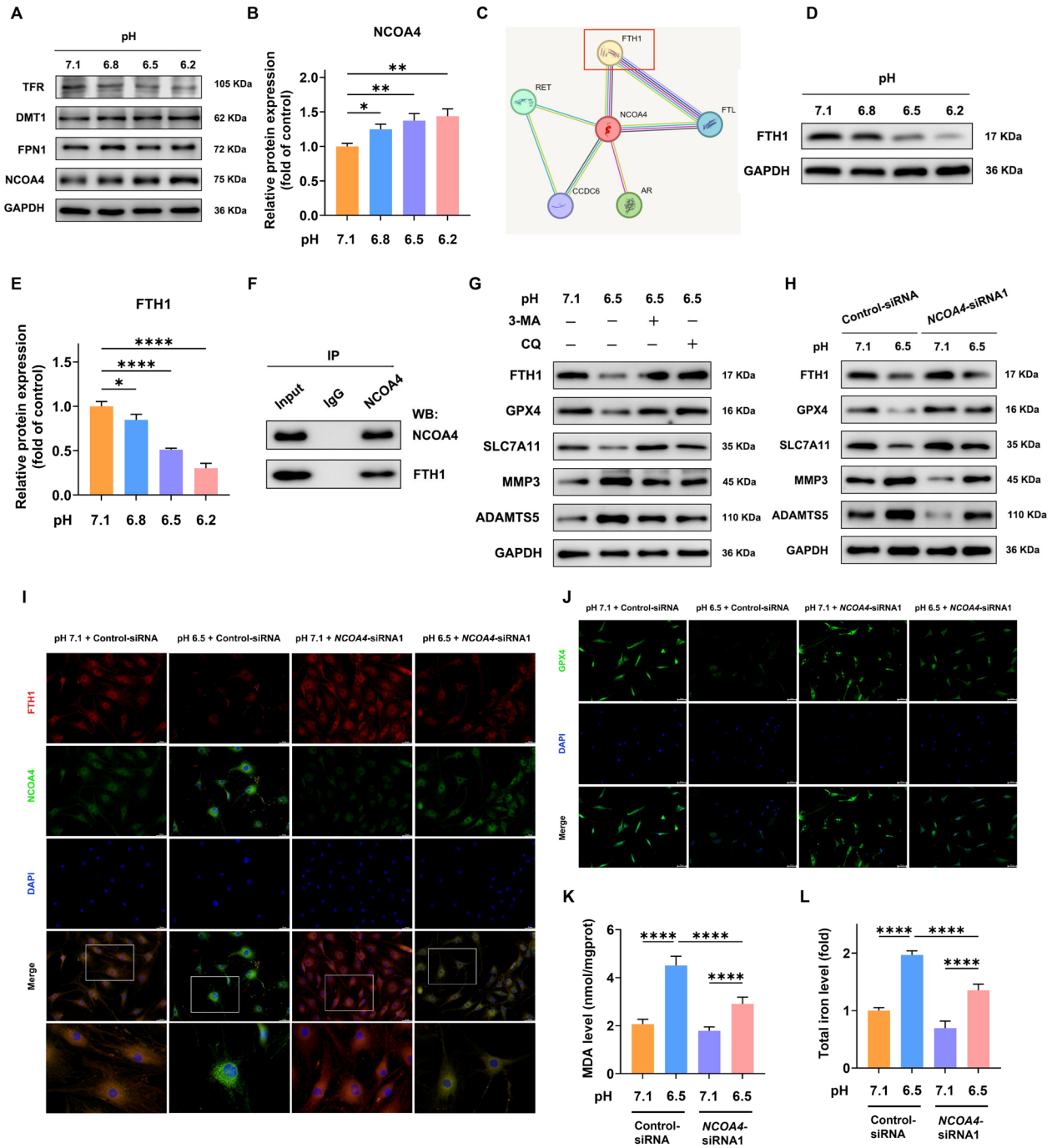

Fig. 4 NCOA4-mediated ferritinophay participated in the acidic-induced ferroptosis in human NPSCs. **A**, **B** Representative western blot images of TFR, DMT1, FPN1, and NCOA4 in the acidic-treated NPSCs. The relative band densities of NCOA4 were quantified. **C** The target prediction of NCOA4 using STRING database. **D**, **E** Representative western blot images of FTH1 in the acidic-treated NPSCs. The relative band densities were quantified. **F** Co-IP analysis of the binding between NCOA4 and FTH1. **G** Representative western blot images of FTH1, GPX4, SLC7A11, MMP3, and ADAMTS5 in NPSCs treated with 3-MA and CQ under acidic condition. **H** Western blot analysis showing the expression levels of FTH1, GPX4, SLC7A11, MMP3, and ADAMTS5 after NPSCs treated with *NCOA4*-siRNA and Control-siRNA under acidic condition. **I** The expression of NCOA4 and FTH1 and their colocalization in NPSCs were determined by immunofluorescence. Nuclei were stained with DAPI. Scale bar: 50 μm. **J** NPSCs were labeled with anti-GPX4 antibodies, and representative fluorescence images are shown. Nuclei were stained with DAPI. Scale bar: 50 μm. **K** Quantification of MDA contents in NPSCs. **L** Total iron levels in NPSCs. A *P*-value less than 0.05 was deemed to be statistically significant. (*$P < 0.05$; **$P < 0.01$; ***$P < 0.001$; ****$P < 0.0001$; ns, not significant)

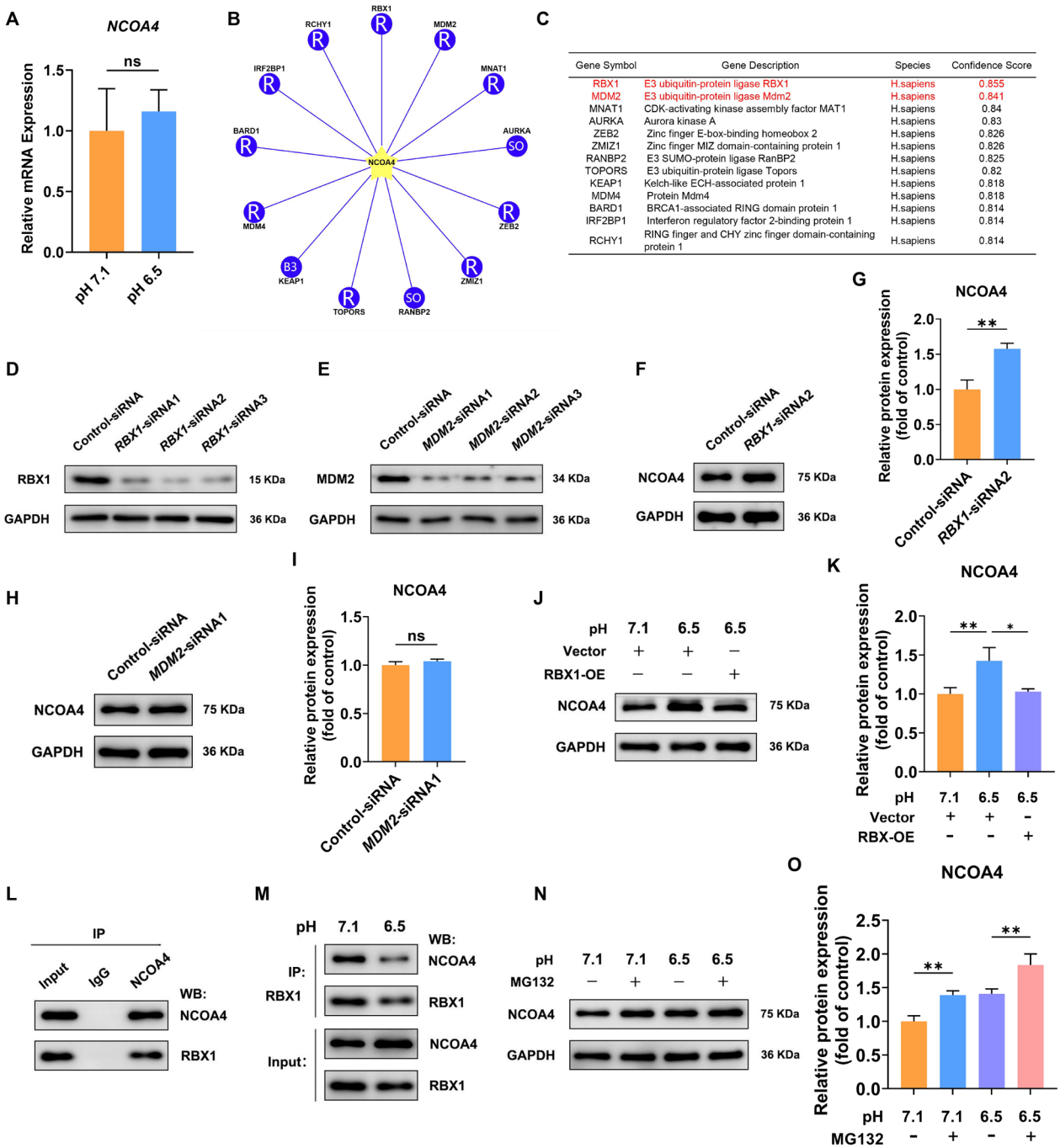

Fig. 5 RBX1-mediated ubiquitination modulates NCOA4 expression. **A** The relative mRNA levels of *NCOA4* in acidic and control groups. **B**, **C** prediction of E3 ligases targeting NCOA4 as substrate using the online tool UbiBrowser. **D**, **E** Stable RBX1-deficient and MDM2-deficient NPSCs were subjected to Western blot analysis to validate the efficiency. **F**, **G** Western blot analysis showing the protein expression level of NCOA4 after NPSCs treated with *RBX1*-siRNA and Control-siRNA. The relative band densities were quantified. **H**, **I** Western blot analysis showing the protein expression level of NCOA4 after NPSCs treated with *MDM2*-siRNA and Control-siRNA. The relative band densities were quantified. **J**, **K** Western blot analysis showing the protein expression level of NCOA4 after NPSCs treated with RBX1 overexpression under acidic condition. The relative band densities were quantified. **L** Co-IP analysis of the binding between NCOA4 and RBX1. **M** NPSCs were treated with acidic condition for 24 h and the Co-IP analysis of the binding between NCOA4 and RBX1 was shown. **N**, **O** Western blot analysis showing the protein expression level of NCOA4 after NPSCs treated with MG132, the proteasome inhibitor. The relative band densities were quantified. A *P*-value less than 0.05 was deemed to be statistically significant. (**P* < 0.05; ***P* < 0.01; ns, not significant)

with NCOA4 were retrieved. Meanwhile, RBX1 and MDM2, which had high confidence scores, might modulate NCOA4 ubiquitination (Fig. 5B and C). We transfected NPSCs with three types of *RBX1*-siRNAs and *MDM2*-siRNAs. According to the outcomes of Western blot, *RBX1*-siRNA2 and *MDM2*-siRNA1 were utilized in subsequent research due to the high knockdown efficiency (Fig. 5D and E and Supplementary Fig. 4A and B). Next, we performed Western blot to further confirm the effects of RBX1 and MDM2 on the expression of NCOA4. The data showed that the inhibition of RBX1, but not MDM2, significantly promoted the expression of NCOA4 (Fig. 5F–I). Additionally, we overexpressed RBX1 in the NPSCs to further confirm the biological effect of RBX1 on NCOA4. Indeed, high expression of RBX1 significantly downregulated NCOA4 expression in an acidic condition (Fig. 5J, K). Therefore, the degradation of NCOA4 proteins might be mediated by the E3 ubiquitin–protein ligase RBX1 in human NPSCs.

To further ascertain the interaction between RBX1 and NOCA4, we performed Co-IP analysis. We found that RBX1 can directly bind to NCOA4 (Fig. 5L). Moreover, we investigated the interaction between RBX1 and NCOA4 under an acidic condition. Co-IP assay revealed that the acidic condition suppressed the interaction between RBX1 and NCOA4 in the NPSCs (Fig. 5M). Given that RBX1 functions as the E3 ubiquitin ligase, we further explored whether NCOA4 is regulated by the ubiquitin–proteasome pathway under an acidic condition and whether RBX1 overexpression-induced reduction in NCOA4 can be ascribed to ubiquitination. After being exposed to an acidic condition, the NPSCs were treated with MG132, which is a proteasome inhibitor. Western blot analysis showed that MG132 can further increase the level of NCOA4 in an acidic condition (Fig. 5N and O). Besides, the Co-IP experiment demonstrated that the overexpression of RBX1 increased the ubiquitination of NCOA4, while the acidic condition decreased ubiquitination of NCOA4 (Supplementary Fig. 4C). To investigate the expression levels of NCOA4 and RBX1 in human local NP tissues during IVDD progression, we collected another three discs with Pfirrmann grade II, three with Pfirrmann grade III, three with Pfirrmann grade IV, and three with Pfirrmann grade V from 12 patients undergoing spinal surgery. Western blot analysis revealed that as the severity of IVDD increased, the levels of NCOA4 were significantly elevated, whereas the levels of RBX1 were markedly reduced in the severely degenerated discs (Supplementary Fig. 4D–F). These results revealed the acidic condition suppresses the interaction between RBX1 and NCOA4, leading to increased NCOA4 protein levels.

Inhibition of RBX1 promotes ferroptosis through NCOA4-mediated ferritinophagy in human NPSCs

To further clarify the role of RBX1 in NOCA4 ubiquitination and associated ferroptosis process, we transfected *RBX1*-siRNA2 into NPSCs and examined the expression of NCOA4 proteins and molecular markers of ferroptosis in human NPSCs. Western blot analyses showed that RBX1 inhibition significantly promoted the expression of NCOA4 and resulted in a high level of ferroptosis (i.e., low expression of FTH1, GPX4 and SLC7A11) under acidic conditions (Fig. 6A–E). Consistently, a deficiency of RBX1 significantly attenuated the MMP of NPSCs under an acidic condition (Fig. 6F and G).

To verify the causality between RBX1 and NCOA4 in NPSCs under an acidic condition, we conducted the co-transfection of *RBX1*-siRNA and *NCOA4*-siRNA into human NPSCs. Indeed, the inhibition of NCOA4 reversed the ferroptosis process (i.e., increased expression of FTH1, GPX4, and SLC7A11) induced by RBX1 deficiency under an acidic condition (Fig. 6H–K). Moreover, the *RBX1* deficiency–induced increases in the levels of MDA and intracellular iron in acid-treated NPSCs was mitigated by *NCOA4* knockdown (Fig. 6L and M). Overall, we concluded that RBX1 deficiency can promote ferroptosis through NCOA4-mediated ferritinophagy in human NPSCs.

AAV-mediated Rbx1 overexpression ameliorates ferroptotic effects on IVDD progression by suppressing NCOA4-mediated ferritinophagy in vivo

Given that RBX1 negatively regulates the ubiquitination of NOCA4 and is essential to acid-induced ferroptosis, we speculated that *Noca4* inhibition or *Rbx1* overexpression might protect iscs from ferroptosis during IVDD. We first established a disc degeneration model through the needle puncture of the tail (Fig. 7A). The AAV-*Rbx1*, AAV-*Ncoa4*, and siRNAs specifically designed to target *Ncoa*, were injected into the disc, and the extent of IVDD in the rats was evaluated through MRI on the basis of the Pfirrmann grading system. The results showed that the signal intensities of the IVD in the needle puncture group treated with *Ncoa4*-siRNA were significantly higher than those treated with only needle puncture, demonstrating that the suppression of NCOA4-mediated ferritinophagy and ameliorated the progression of IVDD in vivo. Besides, the injection of AAV-*Rbx1* after the needle puncture significantly improved the signal intensities of the IVD compared with the needle puncture group. By contrast, the alleviation of the IVDD progression with AAV-*Rbx1* was blocked by AAV-*Rbx1* and AAV-*Ncoa4* after needle puncture, showing that RBX1 ameliorated IVDD by suppressing NCOA4-mediated ferritinophagy (Fig. 7B and C).

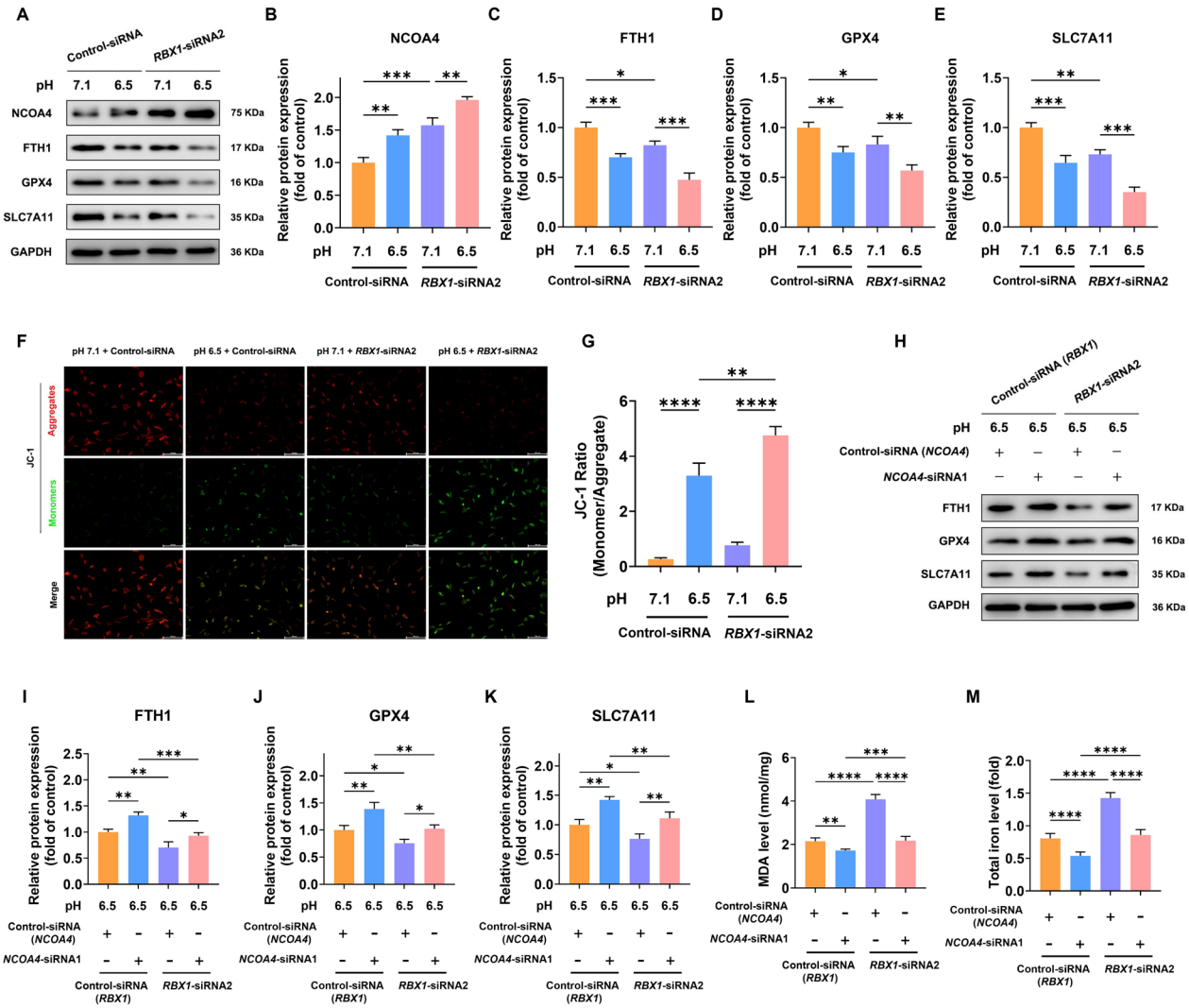

Fig. 6 Inhibition of RBX1 promotes ferroptosis through NCOA4-mediated ferritinophagy in human NPSCs. **A**–**E** Representative western blot images of NCOA4, FTH1, GPX4, and SLC7A11 in NPSCs treated with *RBX1*-siRNA and Control-siRNA under acidic condition for 24 h. The relative band densities were quantified. **F**, **G** JC-1 staining for mitochondrial membrane potential in NPSCs. Scale bar: 200 μm. Quantitative analysis of mitochondrial membrane potential was shown as the ratio of monomer/aggregate. **H**, **K** Representative western blot images of FTH1, GPX4, and SLC7A11 in NPSCs treated with *RBX1*-siRNA, *NCOA4*-siRNA and Control-siRNA under acidic condition for 24 h. The relative band densities were quantified. **L** Quantification of MDA contents in NPSCs. **M** Total iron levels in NPSCs. A *P*-value less than 0.05 was deemed to be statistically significant. (**P* < 0.05; ***P* < 0.01; ****P* < 0.001; *****P* < 0.0001)

(See figure on next page.)

Fig. 7 *Rbx1* overexpression ameliorates ferroptotic effects on IVDD progression via suppressing NCOA4-mediated ferritinophagy in vivo. **A** Schematic illustration depicting the process of constructing the animal model and the subsequent treatments used in this study. **B**, **C** Following 4 weeks of the specified treatments, the degenerated extent of the rat caudal discs was assessed using T2-weighted MRI and the associated Pfirrmann grades were determined. **D** Representative images demonstrating H&E staining and SO staining of midsagittal sections of rat disc specimens. **E** Histological scores of IVDs based on the H&E staining and SO staining; Scale bar: 500 μm. **F** Quantification of MDA contents in different interventions of rat discs; **G** quantification of relative GSH levels in in different interventions of rat discs; a *P*-value less than 0.05 was deemed to be statistically significant. (**P* < 0.05; ***P* < 0.01; ****P* < 0.001; *****P* < 0.0001; ns, not significant)

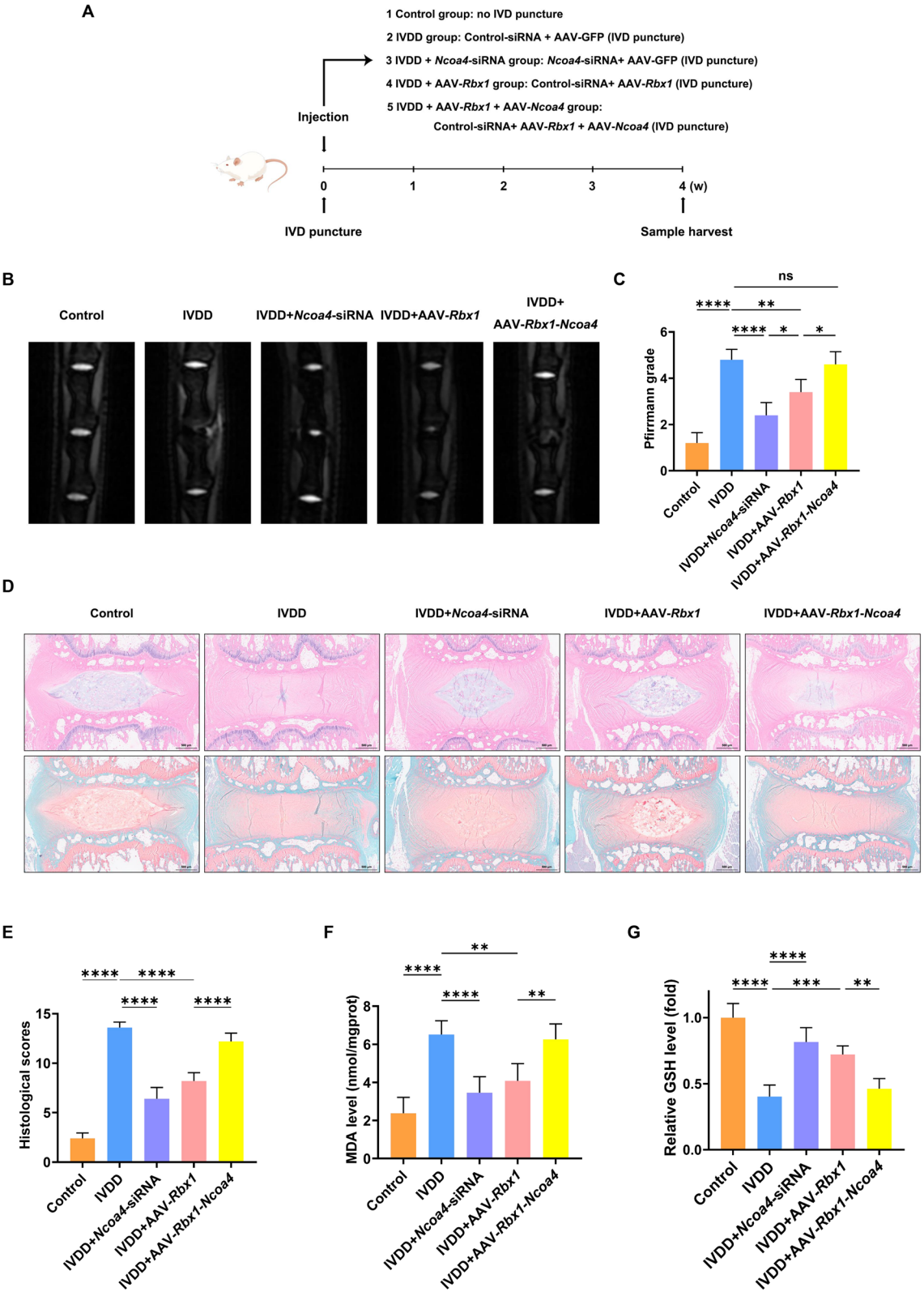

Fig. 7 (See legend on previous page.)

Histological assessments using H&E and SO staining revealed that the IVDs treated with *Ncoa4*-siRNA or AAV-*Rbx1* exhibited decreased degeneration compared with the IVDD group. The *Ncoa4*-siRNA or AAV-*Rbx1*-treated degenerated IVDs showed preserved and well-organized NP tissue structures with star-shaped cells, low degree of tissue fibrillation in the NP area, and distinguishable boundary between NP and AF tissues. However, the injection with AAV-*Ncoa4* after AAV-*Rbx1* treatment blocked the alleviation of IVDD compared with IVDs treated with *Ncoa4*-siRNA or AAV-*Rbx1* (Fig. 7D and E).

Furthermore, the increased levels of MDA and reduced GSH level in the IVDD group were significantly reversed after the injection of *Ncoa4*-siRNA and AAV-*Rbx1*, indicating that the progression of ferroptosis in the rat discs was accompanied by the exacerbation of IVDD, and the inhibition of *Ncoa4* and the overexpression of *Rbx1* inhibited the progression of ferroptosis and IVDD. However, these therapeutic effects were offset by the overexpression of *Ncoa4* (Fig. 7F and G). These results demonstrated that RBX1 suppressed NCOA4-mediated ferritinophagy and ameliorated the ferroptotic effect on IVDD.

Discussion

The dysregulation of iron homeostasis is implicated in numerous age-related diseases [53–55], but the pathological mechanism underlying IVDD remains largely unexplored. Studies investigating the causal link between ferroptosis and IVDD have emerged only recently. Lu et al. [32] employed TBHP to simulate an oxidative stress condition and investigated the regulatory mechanisms involved in ferroptosis-mediated decline in NPCs. They found that ferroportin dysregulation resulted in intercellular iron overload, which can be reversed by the upregulation of MTF1 and the suppression of the JNK pathway. Li et al. [34] demonstrated that TBHP aggravated ferroptosis in NPCs by upregulating ATF3 and inhibiting miR-874-3p. Bin et al. [35] reported that under inflammatory conditions, ferroptosis can be activated by the IL-6/miR-10a-5p/IL-6R axis in cartilage cells. Meanwhile, Yu et al. [36] indicated that inflammatory conditions stimulated by IL-1β can decrease NRF2 expression and upregulate ROS products in NPCs, and circ_0072464 shuttled by bone marrow mesenchymal stem cell–secreted extracellular vesicle diminishes ferroptosis by downregulating miR431 and upregulating NRF2. Furthermore, Wang et al. [37] mimicked iron overload with FAC and found that iron overload was remarkably correlated with the initiation and progression of IVDD and induction of oxidative stress and ferroptosis. These studies demonstrated that NPC ferroptosis can be induced under oxidative stress and in microenvironments with inflammation or iron overload; however, whether an acidic microenvironment, the prominent microenvironmental change observed in IVDD, can trigger ferroptosis remains unclear.

Stem cell–based therapy has emerged as a promising approach for IVDD intervention, and endogenous NPSCs showed great potential in repairing IVD [56]. However, no study has investigated the mechanisms of ferroptosis in NPSCs, particularly the mechanism by which acidic conditions influence iron homeostasis and the stem cell-based repair of degenerated IVD. Therefore, we explored whether ferroptosis in NPSCs can be triggered in an acidic microenvironment that further induces IVDD. Our study elucidated that acidic conditions decreased the viability of NPSCs and ECM degradation through ferroptosis. NCOA4-mediated ferritinophagy was detected in stem cells exposed to acidic microenvironments. Ferroptosis in NPSCs was upregulated by NCOA4-mediated ferritinophagy but downregulated after NCOA4 ubiquitination by the E3 ubiquitin ligase RBX1. Our research highlighted the role of NCOA4-mediated ferritinophagy and the protective effect of RBX1 on intrinsic stem cell–based cellular repair for IVDD (Fig. 8).

Ferritinophagy, a form of selective autophagy targeting the degradation of the iron-storage ferritin protein, is crucial for maintaining iron homeostasis and is primarily mediated by NCOA4, an autophagy cargo receptor [57]. NCOA4 can regulate ferroptosis by directly binding to and degrading FTH1, thereby enhancing ferroptosis sensitivity. Gryzik et al. [58] demonstrated that NCOA4 deficiency abolished ferritinophagy, resulting in increased ferritin levels and decreased lipid peroxidation. As a result, the cells became highly resistant to erastin-induced ferroptosis. Meanwhile, NCOA4 overexpression delayed RSL3-induced cell death, indicating that the ferritin-iron release is contingent on a specific inducing compound. In addition, NCOA4 knockdown remarkably decreased intracellular ferrous iron and MDA levels but increased GSH level [59]. The present study provided important evidence that NCOA4 knockdown by specific siRNA increases FTH1 expression and limits acidic-induced ferroptosis in NPSCs. Moreover, the increased levels of MMP3 and ADAMTS5, which are markers of ECM degradation, were downregulated by NCOA4 knockdown in an acidic microenvironment, demonstrating that ECM degradation involves NCOA4-mediated ferritinophagy.

Autophagy is an essential catabolic process that maintains cell homeostasis by degrading intracellular substrates via the lysosomal pathway in response to environmental stressors. Yang et al. [33] reported that although NCOA4 silencing ameliorates ferroptosis, it

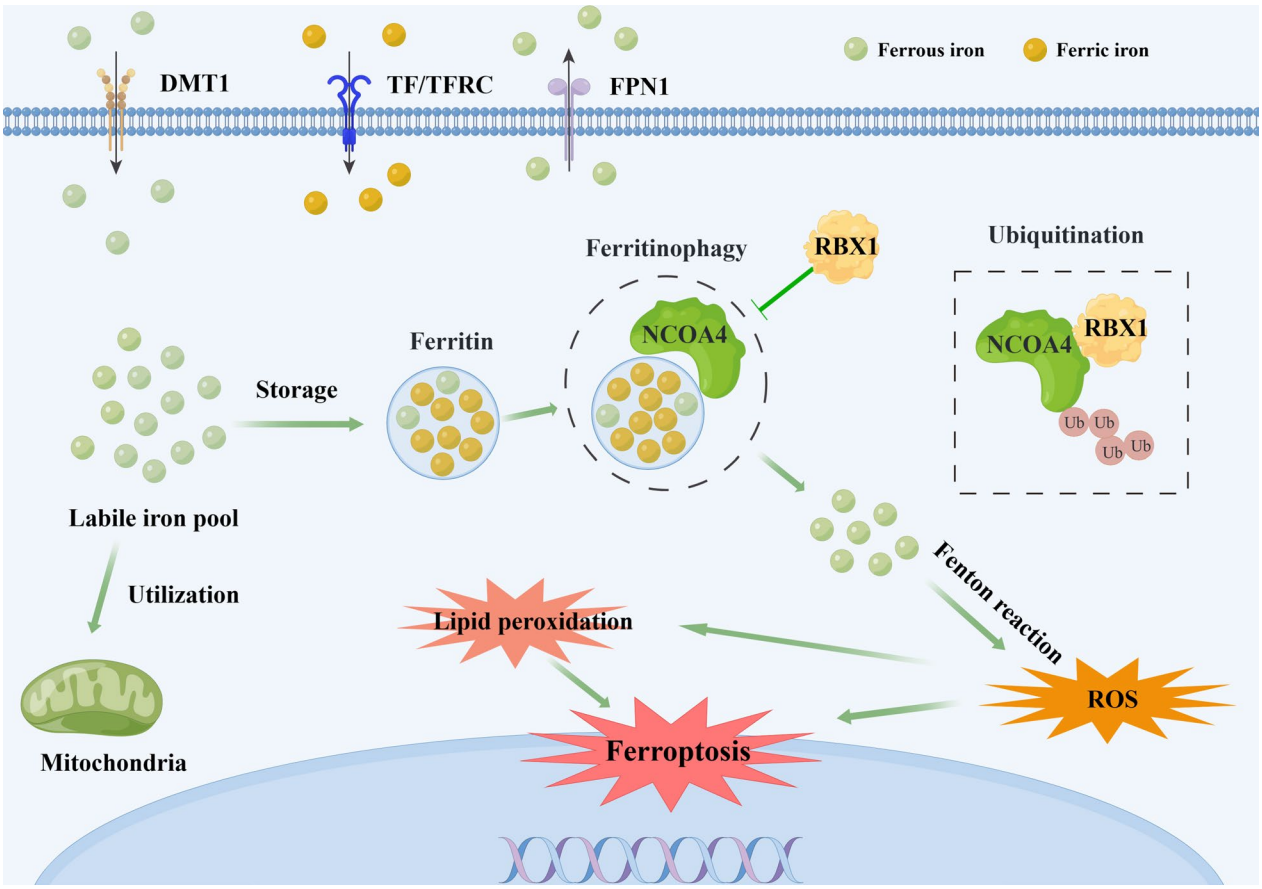

Fig. 8 Schematic illustration indicating the proposed molecular model of RBX1 in regulating NCOA4-mediated ferritinophagy and ferroptosis of human NPSCs. RBX1 directly binds to and ubiquitinates NCOA4, leading to a decrease in NCOA4 expression. This alleviates NCOA4-mediated ferritinophagy, decreases degradation of ferritin, and lowers intracellular iron levels, finally preventing ROS and lipid peroxidation, and inhibiting ferroptosis of human NPSCs. *DMT1* divalentmetal transporter 1, *TF* transferrin, *TFRC* transferrin receptor, *FPN1* ferroportin 1, *NCOA4* Nuclear receptor coactivator 4, *RBX1* Ring-box 1

does not affect autophagy. To further elucidate the role of autophagy in ferritin degradation, we employed two inhibitors (3-MA and CQ) to individually hinder the assembly of autophagosomes and the fusion between autophagosomes and lysosomes. The results showed that ferroptosis and ECM degradation decreased after the inhibition of autophagy in NPSCs treated with the two inhibitors relative to those in NPSCs only subjected to an acidic condition. Thus, autophagic flux blocking can decrease sensitivity of NPSCs to ferroptosis by suppressing NCOA4-mediated ferritinophagy, showing potential as a target for therapeutic interventions for IVDD.

Given that NCOA4 improved the availability of free ferrous iron in the cytosol, we conducted further investigations on the negative inhibition mechanism for ferritinophagy. Sun et al. [60] found that increase in the expression of NCOA4 depends on the JNK-JUN signaling pathway in osteoarthritis. Zhang et al. [46] indicated that COPZ1 knockdown elevated the protein levels of NCOA4 and ultimately contributed to increased ferroptosis in glioblastoma cell lines. Ubiquitination is essential for regulating the post-translational mechanisms of ferroptotic cell death, and numerous studies have emphasized the significance of ubiquitin system enzymes in the regulation of sensitivity to ferroptosis [61]. RBX1 belong to a family of E3 ubiquitin ligases and regulate protein degradation via the ubiquitin–proteasome system [62, 63]. In the current study, we found that the RBX1-mediated ubiquitination of NCOA4 can block ferritinophagy, thereby suppressing ferroptosis. Therefore, RBX1 regulates intracellular iron metabolism and ferroptosis in NPSCs, exhibiting high potential as a therapeutic target for the treatment of IVDD.

Conclusion

For the first time, our study revealed that acidic-induced ferroptosis was involved in NPSC decline and ECM degradation during IVDD. NCOA4-mediated

ferritinophagy resulted in NPSC ferroptosis and aggravated IVDD. RBX1 directly bound to and regulated NCOA4-mediated ferritinophagy and ferroptosis in NPSCs. The inhibition of NCOA4-mediated ferritinophagy provides valuable insights into the potential application of endogenous stem cell-based IVD self-repair and self-regeneration for IVDD treatment.

Supplementary Information

The online version contains supplementary material available at https://doi.org/10.1186/s12967-025-06412-7.

Supplementary Material 1

Supplementary Material 2

Supplementary Material 3. Figure 1.Correlation analyses between iron metabolism indicators and cumulative Pfirrmann grades. The results showed that levels of transferrin and TIBC were not significantly associated with the cumulative Pfirrmann grades.Correlation analyses between iron metabolism indicators and cumulative Pfirrmann grades in female blood samples. The results showed that levels of transferrin and TIBC were not significantly associated with the cumulative Pfirrmann grades. Correlation analyses between iron metabolism indicators and cumulative Pfirrmann grades in male blood samples. The results showed that levels of transferrin and TIBC were not significantly associated with the cumulative Pfirrmann grades.The levels of serum ferritin and UIBC in high cumulative Pfirrmann grades compared to those in low cumulative Pfirrmann grades for samples from female cohorts.The levels of serum ferritin and UIBC in high cumulative Pfirrmann grades compared to those in low cumulative Pfirrmann grades for samples from male cohorts

Supplementary Material 4. Figure 2.The multi-lineage differentiation potency of NPSCs. Lipid droplets in NPSC were stained in sepia with Oil Red O after adipogenic induction. Calcium nodules which were stained in red with Alizarin Red were demonstrated in NPSC after osteogenic induction. The monolayer of NPSC after chondrogenic differentiation induction produced glycosaminoglycan, which was stained in blue with Alcian Blue. Scale bar: 250 μm

Supplementary Material 5. Figure 3.The quantification of relative band densities of TFR, DMT1, and FPN1 in the acidic-treated NPSCs.The quantification of relative band densities of FTH1, GPX4, SLC7A11, MMP3, and ADAMTS5 in NPSCs treated with 3-MA and CQ under acidic condition. Stable NCOA4-deficient NPSCs were subjected to Western blot analysis to validate the efficiency. The relative band densities were quantified.Western blot analysis showing the expression levels of FTH1, GPX4, SLC7A11, MMP3, and ADAMTS5 after NPSCs treated with *NCOA4*-siRNA and Control-siRNA under acidic condition. The relative band densities were quantified. Quantitative analysis of GPX4 was shown as relative fluoresence intensity. Representative fluorescence microscopy photomicrographs of intracellular ROS in NPSCs. Scale bar: 50 μm. Quantitative analysis of intracellular ROS was shown as relative fluoresence intensity. A *P*-value less than 0.05 was deemed to be statistically significant..

Supplementary Material 6. Figure 4.Western blot analysis showing the protein expression level of RBX1 after NPSCs treated with *RBX1*-siRNA1, *RBX1*-siRNA2, *RBX1*-siRNA2, and Control-siRNA. The relative band densities were quantified.Western blot analysis showing the protein expression level of MDM2 after NPSCs treated with MDM2-siRNA1, MDM2-siRNA2, MDM2-siRNA3, and Control-siRNA. The relative band densities were quantified.Co-IP analysis of the binding between NCOA4 and RBX1. The result showing the overexpression of RBX1 increased the ubiquitination of NCOA4, while the acidic condition decreased ubiquitination of NCOA4. Representative western blot images of NCOA4 and RBX1 in NP tissues from Mild- to Severe- IVDD groups. The relative band densities were quantified. A *P*-value less than 0.05 was deemed to be statistically significant..

Author contributions

Cai-Liang Shen, Lu-Ping Zhou, Liang Kang, and Ren-Jie Zhang designed the experiments, oversaw the collection of results and data interpretation, and drafted the article. Lu-Ping Zhou, Liang Kang, Zhi-Gang Zhang, and Chen-Hao Zhao contributed to execution, data acquisition, and interpretation. Lu-Ping Zhou, Liang Kang, Zhi-Gang Zhang, Chen-Hao Zhao, Chong-Yu Jia, Xian-Liang Zhang, and Hua-Qing Zhang performed the experiments. Lu-Ping Zhou, Hua-Qing Zhang, and Ren-Jie Zhang contributed to interpretation. The article was prepared by Lu-Ping Zhou, Liang Kang, Ren-Jie Zhang, and Cai-Liang Shen. All authors have seen and approved the final version.

Funding

This study was supported by the National Natural Science Foundation of China (82272551) and National Natural Science Foundation of China (81772408).

Data availability

The data that support the findings of this study are available from the corresponding author upon reasonable request.

Declarations

Ethics approval and consent to participate

The clinical study and study regarding the collection of human nucleus pulposus tissues were approved by the Ethics Committee of the First Affiliated Hospital of Anhui Medical University. The animal experiments were approved by the Animal Care Committee of Anhui Medical University.

Patient consent statement

Informed consent was obtained from all participants or their legal guardians.

Consent for publication

All authors give their consent to publish if accepted by the Editorial Board.

Competing interests

None of the authors have any conflict of interests.

Author details

[1]Department of Orthopedics and Spine Surgery, The First Affiliated Hospital of Anhui Medical University, 218 Jixi Road, Hefei 230022, Anhui, China. [2]Laboratory of Spinal and Spinal Cord Injury Regeneration and Repair, The First Affiliated Hospital of Anhui Medical University, Hefei 230022, Anhui, China. [3]Anhui Province Research Center for the Clinical Application of Digital Medical Technology, The First Affiliated Hospital of Anhui Medical University, Hefei 230022, Anhui, China.

Received: 15 April 2024 Accepted: 23 March 2025
Published online: 07 May 2025

References

1. Muñoz Laguna J, Puhan MA, Rodríguez Artalejo F, De Pauw R, Wyper GMA, Devleesschauwer B, Santos JV, Hincapié CA. Certainty of the global burden of disease 2019 modelled prevalence estimates for musculoskeletal conditions: a meta-epidemiological study. Int J Public Health. 2023;68:1605763.
2. Guan SY, Zheng JX, Sam NB, Xu S, Shuai Z, Pan F. Global burden and risk factors of musculoskeletal disorders among adolescents and young adults in 204 countries and territories, 1990–2019. Autoimmun Rev. 2023;22: 103361.
3. Vergroesen PP, Kingma I, Emanuel KS, Hoogendoorn RJ, Welting TJ, van Royen BJ, van Dieën JH, Smit TH. Mechanics and biology in intervertebral disc degeneration: a vicious circle. Osteoarthr Cartil. 2015;23:1057–70.
4. Martin BI, Deyo RA, Mirza SK, Turner JA, Comstock BA, Hollingworth W, Sullivan SD. Expenditures and health status among adults with back and neck problems. JAMA. 2008;299:656–64.
5. Zhang W, Li G, Luo R, Lei J, Song Y, Wang B, Ma L, Liao Z, Ke W, Liu H, et al. Cytosolic escape of mitochondrial DNA triggers cGAS-STING-NLRP3

axis-dependent nucleus pulposus cell pyroptosis. Exp Mol Med. 2022;54:129–42.
6. Lyu FJ, Cui H, Pan H, Mc Cheung K, Cao X, Iatridis JC, Zheng Z. Painful intervertebral disc degeneration and inflammation: from laboratory evidence to clinical interventions. Bone Res. 2021;9:7.
7. Vadalà G, Russo F, Di Martino A, Denaro V. Intervertebral disc regeneration: from the degenerative cascade to molecular therapy and tissue engineering. J Tissue Eng Regen Med. 2015;9:679–90.
8. Smith LJ, Nerurkar NL, Choi KS, Harfe BD, Elliott DM. Degeneration and regeneration of the intervertebral disc: lessons from development. Dis Model Mech. 2011;4:31–41.
9. Blanco JF, Graciani IF, Sanchez-Guijo FM, Muntión S, Hernandez-Campo P, Santamaria C, Carrancio S, Barbado MV, Cruz G, Gutierrez-Cosío S, et al. Isolation and characterization of mesenchymal stromal cells from human degenerated nucleus pulposus: comparison with bone marrow mesenchymal stromal cells from the same subjects. Spine (Phila Pa 1976). 2010;35:2259–65.
10. Sakai D, Nakamura Y, Nakai T, Mishima T, Kato S, Grad S, Alini M, Risbud MV, Chan D, Cheah KS, et al. Exhaustion of nucleus pulposus progenitor cells with ageing and degeneration of the intervertebral disc. Nat Commun. 2012;3:1264.
11. Luo R, Li G, Zhang W, Liang H, Lu S, Cheung JPY, Zhang T, Tu J, Liu H, Liao Z, et al. O-GlcNAc transferase regulates intervertebral disc degeneration by targeting FAM134B-mediated ER-phagy. Exp Mol Med. 2022;54:1472–85.
12. Li S, Liao Z, Yin H, Liu O, Hua W, Wu X, Zhang Y, Gao Y, Yang C. G3BP1 coordinates lysophagy activity to protect against compression-induced cell ferroptosis during intervertebral disc degeneration. Cell Prolif. 2022;56: e13368.
13. Liao Z, Wu X, Song Y, Luo R, Yin H, Zhan S, Li S, Wang K, Zhang Y, Yang C. Angiopoietin-like protein 8 expression and association with extracellular matrix metabolism and inflammation during intervertebral disc degeneration. J Cell Mol Med. 2019;23:5737–50.
14. Sakai D, Andersson GB. Stem cell therapy for intervertebral disc regeneration: obstacles and solutions. Nat Rev Rheumatol. 2015;11:243–56.
15. Henriksson HB, Svala E, Skioldebrand E, Lindahl A, Brisby H. Support of concept that migrating progenitor cells from stem cell niches contribute to normal regeneration of the adult mammal intervertebral disc: a descriptive study in the New Zealand white rabbit. Spine (Phila Pa 1976). 2012;37:722–32.
16. Wang F, Shi R, Cai F, Wang YT, Wu XT. Stem cell approaches to intervertebral disc regeneration: obstacles from the disc microenvironment. Stem Cells Dev. 2015;24:2479–95.
17. Zhao K, An R, Xiang Q, Li G, Wang K, Song Y, Liao Z, Li S, Hua W, Feng X, et al. Acid-sensing ion channels regulate nucleus pulposus cell inflammation and pyroptosis via the NLRP3 inflammasome in intervertebral disc degeneration. Cell Prolif. 2021;54: e12941.
18. Zhang H, Li W, Wu Y, Zhang S, Li J, Han L, Chen H, Wang Z, Shen C, Zhang Y, Tao H. Effects of changes in osmolarity on the biological activity of human normal nucleus pulposus mesenchymal stem cells. Stem Cells Int. 2022;2022:1121064.
19. Chu G, Zhang W, Han F, Li K, Liu C, Wei Q, Wang H, Liu Y, Han F, Li B. The role of microenvironment in stem cell-based regeneration of intervertebral disc. Front Bioeng Biotechnol. 2022;10: 968862.
20. Kitano T, Zerwekh JE, Usui Y, Edwards ML, Flicker PL, Mooney V. Biochemical changes associated with the symptomatic human intervertebral disk. Clin Orthop Relat Res. 1993;293:372–7.
21. Ohshima H, Urban JP. The effect of lactate and pH on proteoglycan and protein synthesis rates in the intervertebral disc. Spine (Phila Pa 1976). 1992;17:1079–82.
22. Risbud MV, Guttapalli A, Stokes DG, Hawkins D, Danielson KG, Schaer TP, Albert TJ, Shapiro IM. Nucleus pulposus cells express HIF-1 alpha under normoxic culture conditions: a metabolic adaptation to the intervertebral disc microenvironment. J Cell Biochem. 2006;98:152–9.
23. Ichimura K, Tsuji H, Matsui H, Makiyama N. Cell culture of the intervertebral disc of rats: factors influencing culture, proteoglycan, collagen, and deoxyribonucleic acid synthesis. J Spinal Disord. 1991;4:428–36.
24. Diamant B, Karlsson J, Nachemson A. Correlation between lactate levels and pH in discs of patients with lumbar rhizopathies. Experientia. 1968;24:1195–6.
25. Dixon SJ, Lemberg KM, Lamprecht MR, Skouta R, Zaitsev EM, Gleason CE, Patel DN, Bauer AJ, Cantley AM, Yang WS, et al. Ferroptosis: an iron-dependent form of nonapoptotic cell death. Cell. 2012;149:1060–72.
26. Zhou L-P, Zhang R-J, Jia C-Y, Kang L, Zhang Z-G, Zhang H-Q, Wang J-Q, Zhang B, Shen C-L. Ferroptosis: a potential target for the intervention of intervertebral disc degeneration. Front Endocrinol. 2022;13:1042060.
27. Tang D, Chen X, Kang R, Kroemer G. Ferroptosis: molecular mechanisms and health implications. Cell Res. 2021;31:107–25.
28. Zeng X, An H, Yu F, Wang K, Zheng L, Zhou W, Bao Y, Yang J, Shen N, Huang D. Benefits of iron chelators in the treatment of Parkinson's disease. Neurochem Res. 2021;46:1239–51.
29. Ayton S, Wang Y, Diouf I, Schneider JA, Brockman J, Morris MC, Bush AI. Brain iron is associated with accelerated cognitive decline in people with Alzheimer pathology. Mol Psychiatry. 2020;25:2932–41.
30. Wang D, Liang W, Huo D, Wang H, Wang Y, Cong C, Zhang C, Yan S, Gao M, Su X, et al. SPY1 inhibits neuronal ferroptosis in amyotrophic lateral sclerosis by reducing lipid peroxidation through regulation of GCH1 and TFR1. Cell Death Differ. 2023;30:369–82.
31. Huang Y, Wu B, Shen D, Chen J, Yu Z, Chen C. Ferroptosis in a sarcopenia model of senescence accelerated mouse prone 8 (SAMP8). Int J Biol Sci. 2021;17:151–62.
32. Lu S, Song Y, Luo R, Li S, Li G, Wang K, Liao Z, Wang B, Ke W, Xiang Q, et al. Ferroportin-dependent iron homeostasis protects against oxidative stress-induced nucleus pulposus cell ferroptosis and ameliorates intervertebral disc degeneration in vivo. Oxid Med Cell Longev. 2021;2021:6670497.
33. Yang RZ, Xu WN, Zheng HL, Zheng XF, Li B, Jiang LS, Jiang SD. Involvement of oxidative stress-induced annulus fibrosus cell and nucleus pulposus cell ferroptosis in intervertebral disc degeneration pathogenesis. J Cell Physiol. 2021;236:2725–39.
34. Li Y, Pan D, Wang X, Huo Z, Wu X, Li J, Cao J, Xu H, Du L, Xu B. Silencing ATF3 might delay TBHP-induced intervertebral disc degeneration by repressing NPC ferroptosis, apoptosis, and ECM degradation. Oxid Med Cell Longev. 2022;2022:4235126.
35. Bin S, Xin L, Lin Z, Jinhua Z, Rui G, Xiang Z. Targeting miR-10a-5p/IL-6R axis for reducing IL-6-induced cartilage cell ferroptosis. Exp Mol Pathol. 2021;118: 104570.
36. Yu X, Xu H, Liu Q, Wang Y, Wang S, Lu R, Jiang Y, Kang H, Hu W. circ_0072464 shuttled by bone mesenchymal stem cell-secreted extracellular vesicles inhibits nucleus pulposus cell ferroptosis to relieve intervertebral disc degeneration. Oxid Med Cell Longev. 2022;2022:2948090.
37. Wang W, Jing X, Du T, Ren J, Liu X, Chen F, Shao Y, Sun S, Yang G, Cui X. Iron overload promotes intervertebral disc degeneration via inducing oxidative stress and ferroptosis in endplate chondrocytes. Free Radic Biol Med. 2022;190:234–46.
38. Chen X, Li J, Kang R, Klionsky DJ, Tang D. Ferroptosis: machinery and regulation. Autophagy. 2021;17:2054–81.
39. Santana-Codina N, Mancias JD. The role of NCOA4-mediated ferritinophagy in health and disease. Pharmaceuticals (Basel). 2018;11:114.
40. Liu J, Kuang F, Kroemer G, Klionsky DJ, Kang R, Tang D. Autophagy-dependent ferroptosis: machinery and regulation. Cell Chem Biol. 2020;27:420–35.
41. Pfirrmann CW, Metzdorf A, Zanetti M, Hodler J, Boos N. Magnetic resonance classification of lumbar intervertebral disc degeneration. Spine (Phila Pa 1976). 2001;26:1873–8.
42. Song Y, Li S, Geng W, Luo R, Liu W, Tu J, Wang K, Kang L, Yin H, Wu X, et al. Sirtuin 3-dependent mitochondrial redox homeostasis protects against AGEs-induced intervertebral disc degeneration. Redox Biol. 2018;19:339–53.
43. Wang J, Nisar M, Huang C, Pan X, Lin D, Zheng G, Jin H, Chen D, Tian N, Huang Q, et al. Small molecule natural compound agonist of SIRT3 as a therapeutic target for the treatment of intervertebral disc degeneration. Exp Mol Med. 2018;50:1–14.
44. Ellidag HY, Eren E, Akdag M, Giray O, Kiraz K, Yilmaz N. The relationship between serum ferritin levels and serum lipids and HDL function with respect to age and gender. Ukr Biochem J. 2016;88:76–86.
45. Li W, Li W, Wang Y, Leng Y, Xia Z. Inhibition of DNMT-1 alleviates ferroptosis through NCOA4 mediated ferritinophagy during diabetes myocardial ischemia/reperfusion injury. Cell Death Discov. 2021;7:267.

46. Zhang Y, Kong Y, Ma Y, Ni S, Wikerholmen T, Xi K, Zhao F, Zhao Z, Wang J, Huang B, et al. Loss of COPZ1 induces NCOA4 mediated autophagy and ferroptosis in glioblastoma cell lines. Oncogene. 2021;40:1425–39.
47. Bibby SR, Jones DA, Ripley RM, Urban JP. Metabolism of the intervertebral disc: effects of low levels of oxygen, glucose, and pH on rates of energy metabolism of bovine nucleus pulposus cells. Spine (Phila Pa 1976). 2005;30:487–96.
48. Han B, Wang H, Ye C, Tao Y, Li H, Liang C, Chen G, Li F, Chen Q. Influence of acidity microenvironment of degenerative intervertebral disc on nucleus pulpous ▪ derived mesenchymal stem cells and adipose—derived mesenchymal stem cells. Chin J Orthop. 2015;35:1243–52.
49. Han B, Wang HC, Li H, Tao YQ, Liang CZ, Li FC, Chen G, Chen QX. Nucleus pulposus mesenchymal stem cells in acidic conditions mimicking degenerative intervertebral discs give better performance than adipose tissue-derived mesenchymal stem cells. Cells Tissues Organs. 2014;199:342–52.
50. Szklarczyk D, Kirsch R, Koutrouli M, Nastou K, Mehryary F, Hachilif R, Gable AL, Fang T, Doncheva NT, Pyysalo S, et al. The STRING database in 2023: protein-protein association networks and functional enrichment analyses for any sequenced genome of interest. Nucleic Acids Res. 2023;51:D638-d646.
51. Li Y, Xie P, Lu L, Wang J, Diao L, Liu Z, Guo F, He Y, Liu Y, Huang Q, et al. An integrated bioinformatics platform for investigating the human E3 ubiquitin ligase-substrate interaction network. Nat Commun. 2017;8:347.
52. Wang X, Li Y, He M, Kong X, Jiang P, Liu X, Diao L, Zhang X, Li H, Ling X, et al. UbiBrowser 2.0: a comprehensive resource for proteome-wide known and predicted ubiquitin ligase/deubiquitinase-substrate interactions in eukaryotic species. Nucleic Acids Res. 2022;50:D719–28.
53. Hu Y, Wang Y, Liu S, Wang H. The potential roles of ferroptosis in pathophysiology and treatment of musculoskeletal diseases-opportunities, challenges, and perspectives. J Clin Med. 2023;12:2125.
54. Stockwell BR, Friedmann Angeli JP, Bayir H, Bush AI, Conrad M, Dixon SJ, Fulda S, Gascón S, Hatzios SK, Kagan VE, et al. Ferroptosis: a regulated cell death nexus linking metabolism, redox biology, and disease. Cell. 2017;171:273–85.
55. Sun Y, Xia X, Basnet D, Zheng JC, Huang J, Liu J. Mechanisms of ferroptosis and emerging links to the pathology of neurodegenerative diseases. Front Aging Neurosci. 2022;14: 904152.
56. He R, Wang Z, Cui M, Liu S, Wu W, Chen M, Wu Y, Qu Y, Lin H, Chen S, et al. HIF1A Alleviates compression-induced apoptosis of nucleus pulposus derived stem cells via upregulating autophagy. Autophagy. 2021;17:3338–60.
57. Mancias JD, Wang X, Gygi SP, Harper JW, Kimmelman AC. Quantitative proteomics identifies NCOA4 as the cargo receptor mediating ferritinophagy. Nature. 2014;509:105–9.
58. Gryzik M, Asperti M, Denardo A, Arosio P, Poli M. NCOA4-mediated ferritinophagy promotes ferroptosis induced by erastin, but not by RSL3 in HeLa cells. Biochim Biophys Acta Mol Cell Res. 2021;1868: 118913.
59. Hou W, Xie Y, Song X, Sun X, Lotze MT, Zeh HJ 3rd, Kang R, Tang D. Autophagy promotes ferroptosis by degradation of ferritin. Autophagy. 2016;12:1425–8.
60. Sun K, Hou L, Guo Z, Wang G, Guo J, Xu J, Zhang X, Guo F. JNK-JUN-NCOA4 axis contributes to chondrocyte ferroptosis and aggravates osteoarthritis via ferritinophagy. Free Radical Biol Med. 2023;200:87–101.
61. Meng Y, Sun H, Li Y, Zhao S, Su J, Zeng F, Deng G, Chen X. Targeting ferroptosis by ubiquitin system enzymes: a potential therapeutic strategy in cancer. Int J Biol Sci. 2022;18:5475–88.
62. Gu J, Chen J, Xiang S, Zhou X, Li J. Intricate confrontation: Research progress and application potential of TRIM family proteins in tumor immune escape. J Adv Res. 2023;54:147–79.
63. Huang N, Sun X, Li P, Liu X, Zhang X, Chen Q, Xin H. TRIM family contribute to tumorigenesis, cancer development, and drug resistance. Exp Hematol Oncol. 2022;11:75.

Publisher's Note